Scintigraphy of the Liver, Spleen, and Biliary Tree

7

Lionel S. Zuckier and Leonard M. Freeman

7.1 Brief Introduction and Historical Perspective

Nuclear medicine occupies a unique niche among various imaging modalities by virtue of its ability to probe functional and physiologic parameters in a noninvasive and quantitative manner. Although at one time scintigraphic studies were used as primary modalities to address anatomic questions, these tasks are currently performed by higher-resolution modalities such as ultrasound (US), computed tomography (CT), and magnetic resonance (MR) imaging. In current practice, nuclear medicine retains a more limited though unique role in the functional and physiologic characterization of tissue [1].

Within the solid gastrointestinal (GI) tract, colloid imaging of the liver visualizes the distribution of reticuloendothelial (RE) system cells which phagocytize intravascular particulate material from the blood, while hepatobiliary scintigraphy evaluates the uptake and excretion of bile-like radiopharmaceuticals by hepatocytes. Specific radiopharmaceuticals such as ^{18}F-FDG, ^{123}I- or ^{131}I-MIBG, ^{67}Ga-gallium citrate, ^{111}In-octreotide, and ^{68}Ga-DOTATATE are used to evaluate metabolic and receptor characteristics of tissues relevant to various pathological processes that affect the liver and spleen. Radiolabeled red blood cells (RBCs) are used to quantitate the blood flow and intravascular blood pool within the liver, helpful when confirming the diagnosis of intrahepatic hemangioma. These applications are summarized in Table 7.1 and will be featured in the chapter below. The role of nuclear medicine tests in evaluating of malignant processes in the liver will be covered elsewhere in this book.

7.2 Biliary Excretion

The initial indication for biliary scintigraphy, to evaluate the etiology of acute right upper quadrant pain, remains current today. A second indication for this technique is the noninvasive evaluation of bile flow to assess extravasation or obstruction in the postsurgical and post-traumatic patient. A third application, which has seen increasing use, is the functional assessment of the gall bladder and biliary tree, so-called biliary kinetics.

L. S. Zuckier (✉) · L. M. Freeman
Division of Nuclear Medicine, Department of Radiology, Montefiore Medical Center, Bronx, NY, USA

Albert Einstein College of Medicine, Bronx, NY, USA
e-mail: Lzuckier@montefiore.org; Lfreeman@montefiore.org

H. Ahmadzadehfar et al. (eds.), *Clinical Nuclear Medicine*,
https://doi.org/10.1007/978-3-030-39457-8_7

Table 7.1 Physiological correlates of radiopharmaceutical behavior in the liver

Radiopharmaceutical	Parameter	Physiologic correlate
^{99m}Tc-sulfur colloid	Uptake	Kupffer cell function
^{99m}Tc-HIDA	Uptake	Hepatocyte function
^{99m}Tc-HIDA	Liver washout	Presence of biliary radicals
^{99m}Tc-red blood cells	Visualization on flow images	Hepatic artery supply
^{99m}Tc-red blood cells	Visualization on delayed images	Intravascular volume
^{133}Xe gas	Uptake	Lipid solubility
^{67}Ga-citrate	Uptake	Transferrin binding
^{111}In-Octreoscan	Uptake	Somatostatin (sstr2) receptor
^{123}I- or ^{131}I-MIBG	Uptake	Catecholamine-producing cells
^{68}Ga-DOTATATE[a]	Uptake	Somatostatin (sstr2) receptor
^{18}F-FDG[a]	Uptake	(glut) transporter

[a]PET based

7.2.1 Radiopharmaceuticals

Attributes of an ideal radiopharmaceutical for evaluation of bile flow include labeling with a radionuclide of favorable imaging and dosimetry characteristics, rapid liver extraction and transit into the biliary system, little or no absorption from the intestine, and minimal renal excretion [2]. ^{99m}Tc-labeled iminodiacetic acid (IDA) derivatives approach these ideal criteria. Typically, 111–185 MBq (3–5 mCi) of ^{99m}Tc-disofenin (2,6-diisopropylacetanilido-iminodiacetic acid) or ^{99m}Tc-mebrofenin (bromo-2,4,6-trimethylacetanilido-iminodiacetic acid) analogs are used for biliary scintigraphy in an adult; the latter has an advantage of superior liver extraction and is therefore favored in patients with more severe hepatic dysfunction. While the IDA analogs generally resemble bilirubin in their uptake and excretion, they are not conjugated as is bilirubin.

7.2.2 Methodology

Clinical information of relevance prior to a hepatobiliary study includes history of previous surgeries, recent bilirubin and liver enzyme levels, and current medications, with special attention to opioids which increase the sphincter of Oddi tone and thereby alter biliary kinetics. Time of most-recent food ingestion is also important as eating profoundly alters biliary kinetics and the pattern of gallbladder (GB) filling.

For evaluation of right upper quadrant pain, patients are generally imaged after a preferably 6-h period of fasting, designed to avoid postprandial contraction of the GB. Patients who are on total parenteral nutrition or have not eaten for over 24 h may have tumefactive bile ("sludge") in the GB which also impedes GB filling. In this situation, a 15-min IV injection of 20 ng/kg of sincalide (CCK-8, the terminal octapeptide of cholecystokinin) given 30 min prior to radiopharmaceutical (Table 7.2) will serve to contract and empty the GB, allowing for subsequent filling with IDA [5]. Interference by opioids can be minimized by delaying the study for a time corresponding to four half-lives of the medication following prior administration [6].

Radiopharmaceutical is injected intravenously, and anterior images over the liver and upper abdomen are obtained at intervals of 5 min or less using a large-field-of-view gamma-camera. Wherever possible, continuous computer acquisition, at approximately one frame per minute, is obtained for subsequent presentation of the data in cine mode. In traditional protocols, imaging is continued for up to 4 h postinjection, until the bowel and GB are visualized or no significant activity remains within the liver (Fig. 7.1). On rare occasions, such as when hepatic uptake is impaired, delayed imaging, up to 24 h, may be helpful.

Table 7.2 Pharmacologic interventions in biliary scintigraphy (after [3] and [4])

Drug	Dose, route	Mechanism	Use
Cholecystokinin-8	20 ng/kg, IV	Stimulates contraction of the GB and relaxes sphincter of Oddi	1. Evacuation of sludge from the GB prior to study, given over 15 min, 30 min prior to radiopharmaceutical 2. Evaluation of percent GB emptying poststimulus (ejection fraction), given over 60 min concurrent with imaging
Morphine sulfate	40 μg/kg or a 2 mg dose slowly over 2–3 min, IV	Constricts sphincter of Oddi	Diverts IDA from the CBD into GB, thereby reducing period of biliary scintigraphy
Phenobarbital	5 mg/kg daily in two divided doses × 5 days, PO	Induces hepatic enzymes	Used to promote liver excretion of IDA in differentiation of neonatal hepatitis from biliary atresia

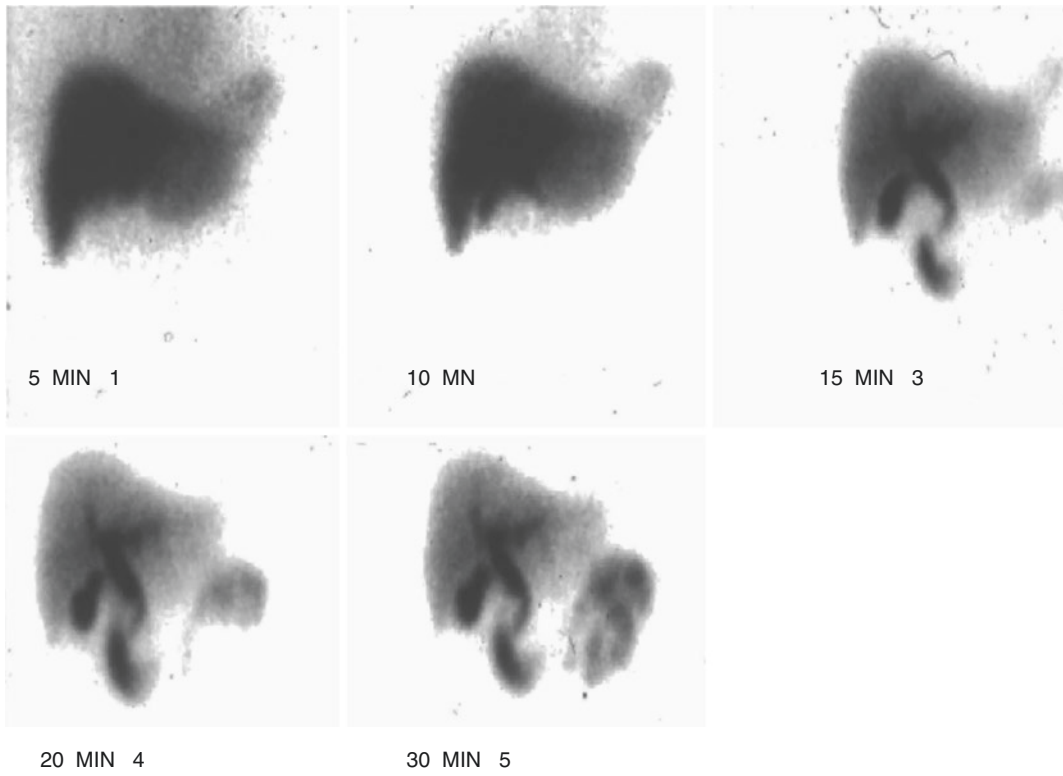

Fig. 7.1 Normal biliary excretion study in a 43-year-old man with acute abdominal pain. Prompt uptake and excretion of radiotracer into the bowel is noted. The gallbladder also fills promptly establishing cystic duct patency, ruling out acute cholecystitis with a greater than 90% accuracy

Rather than continuing the study through 4 h, an alternate accelerated method of biliary scintigraphy can be performed if by 1 h activity is noted within the duodenum but no GB is evident. A quantity of 40 μg/kg or a standard 2 mg dose of morphine sulfate is administered intravenously over 2–3 min (Table 7.2) [6]. This serves to constrict the sphincter of Oddi, thereby shunting bile into the GB (Fig. 7.2). Imaging is terminated 30–60 min following morphine administration, which is functionally equivalent to continuing through the standard 4-h period.

At times it may be difficult to ascertain if a collection of activity medially placed in the

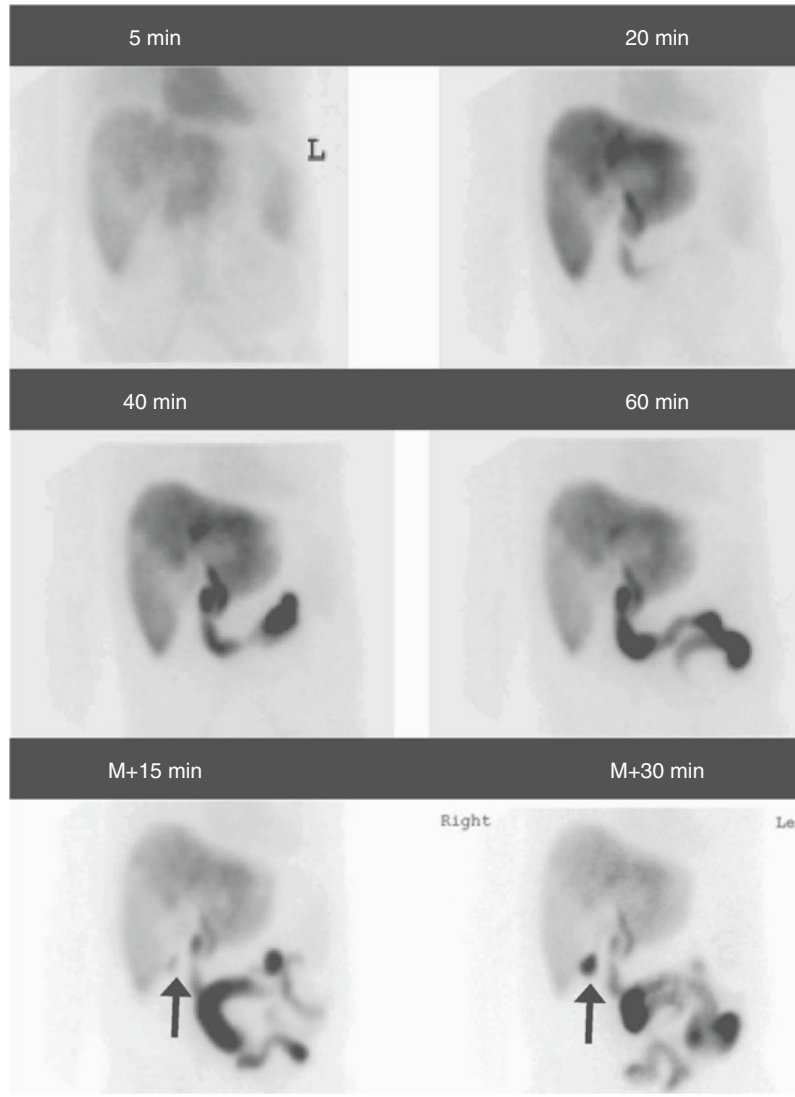

Fig. 7.2 Morphine-augmented cholescintigraphy in a 53-year-old male with history of gallstones and right upper quadrant pain. Imaging through 1 h demonstrated prolonged cardiac blood pool activity and slightly inhomogeneous uptake within the liver, consistent with a known history of liver dysfunction. Increasing activity is noted in the bowel between 20 min and 1 h. At this juncture, 2 mg of morphine sulfate was administrated intravenously, and additional images were obtained, demonstrating filling of the GB (arrows). These findings indicate chronic (but not acute) cholecystitis

right upper quadrant is related to the bowel or in fact is contained within the GB. In addition to obtaining oblique views which may be helpful, patients can be imaged following ingestion of a small amount of water. This serves to wash out the activity within the duodenum but would not affect activity in the GB (Fig. 7.3). SPECT and especially SPECT-CT can also be used to accurately localize ambiguous collections of activity.

7.2.3 Clinical Indications and Interpretation

In the normal patient, hepatic uptake of a ^{99m}Tc-labeled iminodiacetic acid derivative is prompt, with observable blood pool activity in the heart clearing by 5 min postinjection. There is likewise rapid excretion of radiopharmaceutical by the liver, through the biliary tree, and into the duodenum and GB, both of which visualize

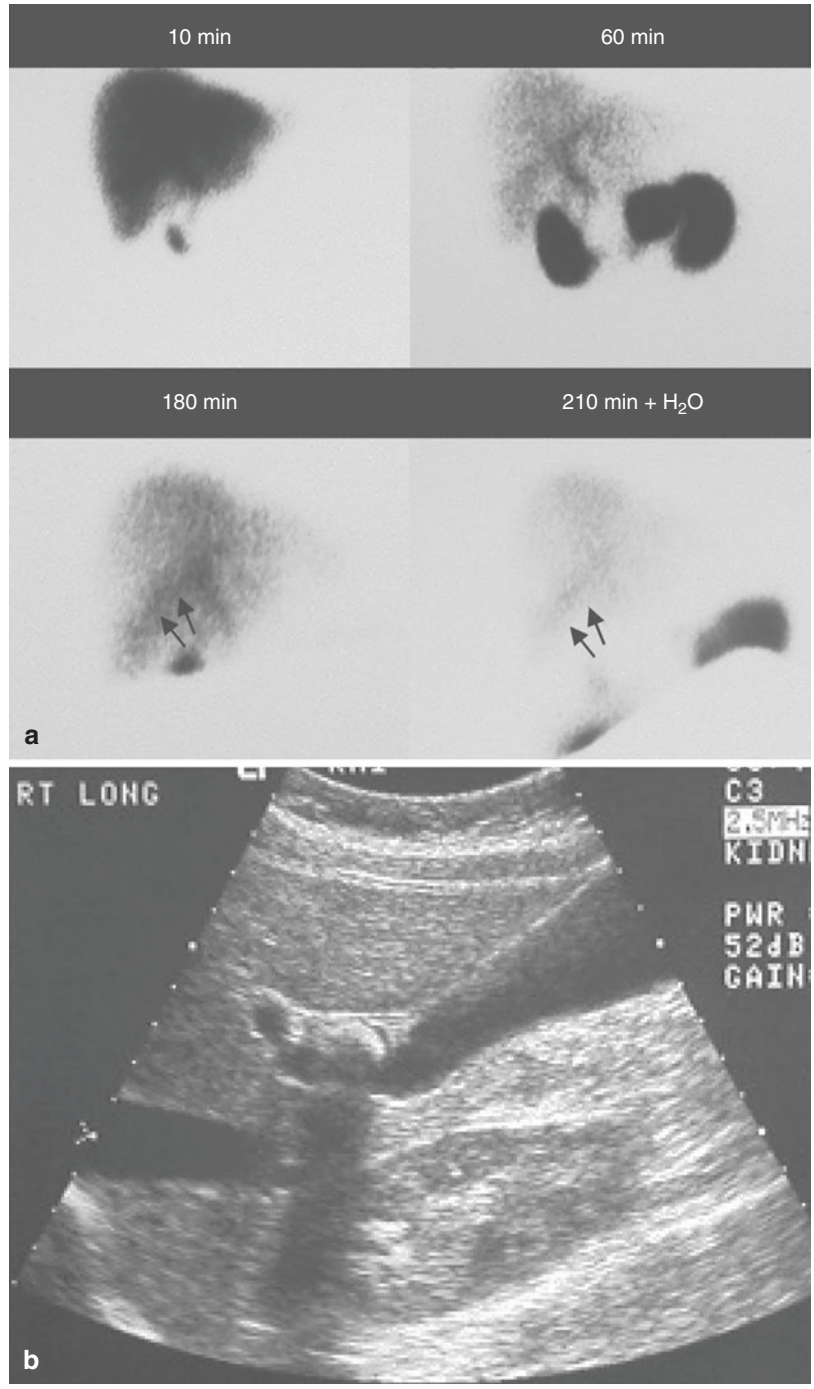

Fig. 7.3 Acute cholecystitis in a 27-year-old woman who presented with right upper quadrant pain. Biliary excretion study (**a**) reveals prompt uptake by the liver and rapid excretion into the small bowel with no visualization of the GB through 3½ h. Of note, there is a suggestion of a faint "stripe" of activity in the region of the GB fossa (arrows), suggesting acute gangrenous cholecystitis. To eliminate the confounding possibility of duodenal activity adjacent to the GB fossa, water was given to the patient following the 3-h view. Additionally, the bowel is shielded by a lead cape on the 3½-h view. Ultrasound study (**b**) demonstrates stones in the region of the neck of the GB (Reprinted from Zuckier and Freeman 2003 with permission)

within the first hour (Fig. 7.1). Transient reflux of activity into the stomach may be seen and a small amount of activity is frequently noted in the urinary tract. Over time, activity proceeds distally into the small and large bowel, while the liver activity diminishes to background levels. Criteria of evaluation include the rate of uptake and excretion of the radiotracer by the liver, the timing of visualization of the bowel and GB, and the appearance of abnormal collections of activ-

ity within the abdomen. Deviations from the norm are associated with various disease states, as described below.

7.2.3.1 Disorders of Hepatic Uptake and Excretion into the Bowel

Uptake by the liver may be impaired, evidenced by slow clearance of the blood pool and increased vicarious excretion of radiopharmaceutical by the kidneys. This abnormality may be primary, due to parenchymal disease such as hepatitis, or secondary, due to obstruction at the level of the common hepatic or common bile duct (CBD). At times it may be difficult to distinguish between intrinsic hepatic disease and obstruction as in both cases activity is retained in the liver and does not proceed distally into the bowel (Fig. 7.4).

In hepatitis, impairment of hepatic uptake and excretion is variable. In mild dysfunction, decreased liver extraction may be evidenced by prolongation of blood pool activity (typically beyond 5 min) and an increase in vicarious excretion by the kidneys. In patients with severe dysfunction, liver uptake may be diminished to the point where the liver is poorly defined, and no biliary excretion is noted. Generally, performance of hepatobiliary studies in patients with total bilirubin above 15–20 mg/dl is of little value in that insufficient activity will be excreted into the biliary tree to yield information regarding its patency. Instances where uptake of radiopharmaceutical by the liver is relatively preserved in contrast to severely decreased hepatic excretion may be rarely seen as an idiosyncratic reaction to medications such as isoniazid and halothane. This unusual combination is termed "intrahepatic cholestasis" and can be confused with relatively acute high-grade mechanical obstruction of the biliary tree.

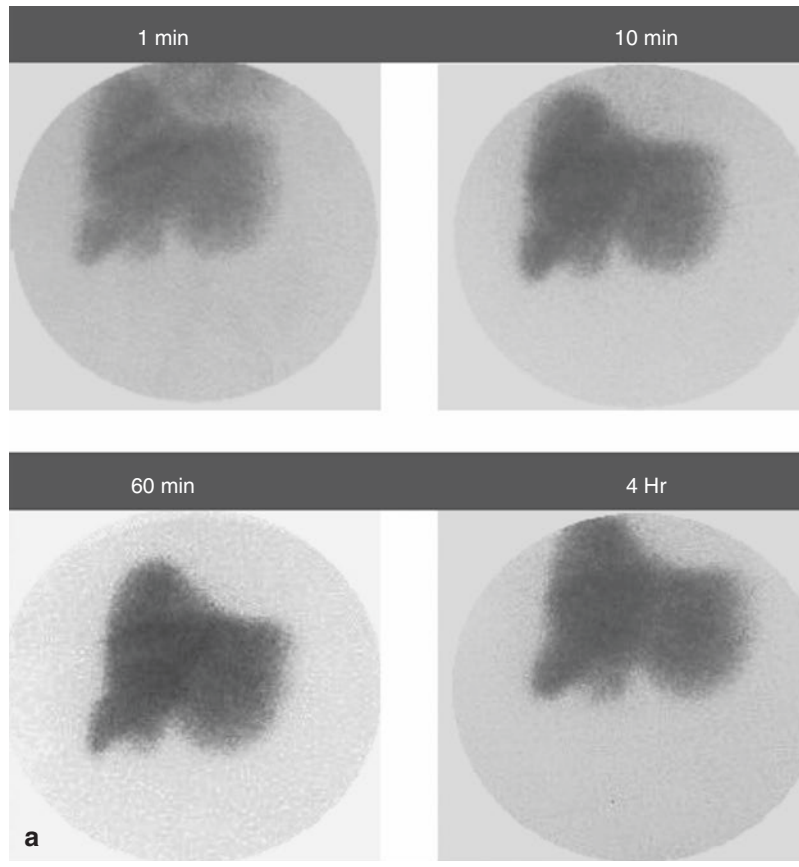

Fig. 7.4 Common bile duct obstruction in a woman who presented with right upper quadrant pain and with suspicion of acute cholecystitis. A fixed "hepatogram" pattern is present through 4 h (**a**), consistent with the diagnosis of CBD obstruction. Correlative ultrasound performed the following day (**b**) demonstrates mild dilation of the CBD to a diameter of 10.7 mm (Reprinted from Zuckier and Freeman 2003 with permission)

Fig. 7.4 (continued)

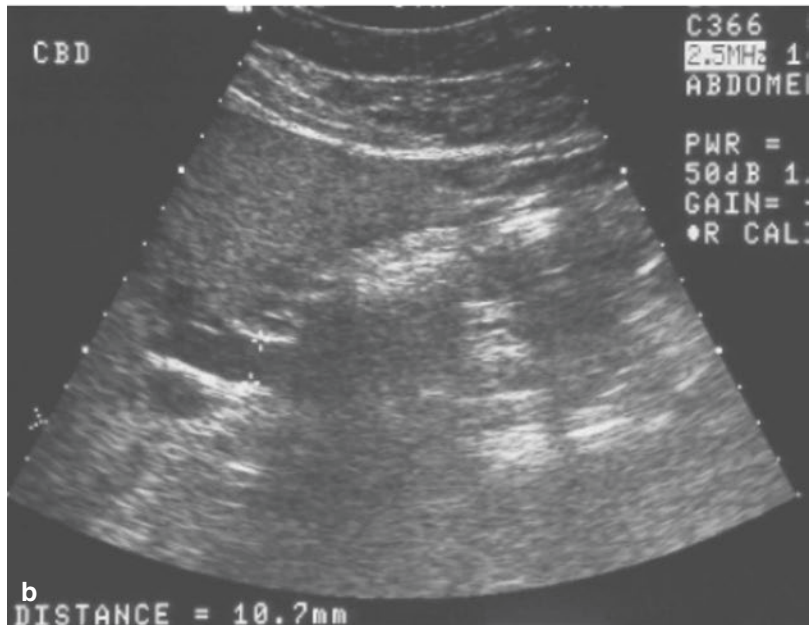

In very early mechanical obstruction of the biliary tree, liver uptake and excretion remain intact, and excreted activity may be observed within the dilated biliary tree to the level of obstruction. As high-grade obstruction of the biliary tree progresses over hours to days, from acute to subacute and chronic, liver uptake and excretion of radiopharmaceutical become increasingly impaired to the point where no activity is observed in the bile ducts, which can even appear as linear photon deficiencies. With prolonged obstruction, the degree of hepatic dysfunction becomes profound, no activity is excreted into the ducts, and it is impossible to differentiate mechanical obstruction from hepatitis.

When partial CBD obstruction is present, ductal prominence and stasis as well as delayed biliary to bile transit may occur, with appearance of activity with the bowel delayed to beyond 60 min. This latter finding is nonspecific and can be seen with a variety of intra-abdominal pathologies as well as following opioid administration or in patients administered CCK-8 prior to scintigraphy [7]. Chronic cholecystitis may also be associated with this finding in some cases.

7.2.3.2 Disorders of Gallbladder Visualization

The primary parameter evaluated on IDA scanning in patients with right upper quadrant pain and suspected cholecystitis is filling of the GB. Assuming sufficient radiotracer reaches the bowel, the GB normally fills between 10 min and 1 h postinjection of radiopharmaceutical. Delayed visualization, between 1 and 4 h, is most commonly ascribed to chronic cholecystitis. Complete non-visualization through 4 h in an acutely ill patient is both highly sensitive and specific for acute cholecystitis, reflecting cystic duct obstruction [8]. This is usually caused by impaction of a stone in the cystic duct; however, acute acalculous cholecystitis will also cause non-visualization of the GB [9]. A recent systematic review and meta-analysis has indicated that cholescintigraphy has the highest diagnostic accuracy of all imaging modalities in the detection of acute cholecystitis [10]. It should be cautioned that in the presence of CBD obstruction or severe hepatic dysfunction, non-visualization of the GB is not diagnostic as there is insufficient flow of activity into the bowel to make any determination of cystic duct patency.

The morphine-enhanced IDA study, as discussed above, shortens the total examination time to 1.5 h instead of the 4 h needed to reliably differentiate acute from chronic cholecystitis. Filling of the GB within 30 min following morphine is analogous to delayed visualization on a 4-h study and suggests chronic cholecystitis (Fig. 7.2). If no filling of the GB occurs by 30 min post-administration of morphine, the cystic duct is demonstrated to be obstructed, consistent with the diagnosis of acute cholecystitis [11, 12].

An important finding, suggestive of complicated acute cholecystitis, is the "rim" or "stripe" sign which consists of a band of increased activity at the lower margin of the liver in the region of the GB fossa (Fig. 7.3). This finding is postulated as being due to adjacent cholestasis in inflamed regional hepatocytes or to actual leakage from a GB perforation. When present, the rim sign has high specificity for complicated acute cholecystitis and predicts increased morbidity [13, 14].

7.2.3.3 Functional Disorders of the Gallbladder [15]

In patients with biliary colic and biliary dyskinesia, routine biliary scintigraphy may be normal. In these cases, an additional provocative test may be necessary to confirm suspected pathology. In one such technique, radiopharmaceutical is administered, and the GB is allowed to fill for 60 min at which point CCK-8 is administered intravenously (Table 7.2) to elicit GB emptying. While various protocols for gallbladder emptying had previously been employed, a multicenter trial conclusively established superiority of a 60-min infusion of 0.02 mg of sincalide per kilogram, with emptying quantified at 60 min [16] (Fig. 7.5). In normal patients, a decrease of activity within the GB of greater than 38% is observed, while in patients with biliary dyskinesia, the GB ejection fraction (EF) remains lower. In instances where CCK-8 is not available, a situation which has occurred periodically, standardized fatty meals have been used to stimulate GB contraction [17, 18]. It must be remembered that physiologic quantitative studies are complicated and must be interpreted within the entire clinical context including pharmacologic effects of other medications [19].

Occasionally, right upper quadrant pain persists following cholecystectomy. In these circumstances, quantitative scintigraphy may be used to assess the physiologic transit of radiotracer from the liver to the bowel, thereby evaluating function of the sphincter of Oddi. Scoring systems have been proposed as a means of objectively and noninvasively predicting which patients would benefit from sphincterotomy (Fig. 7.6) [20].

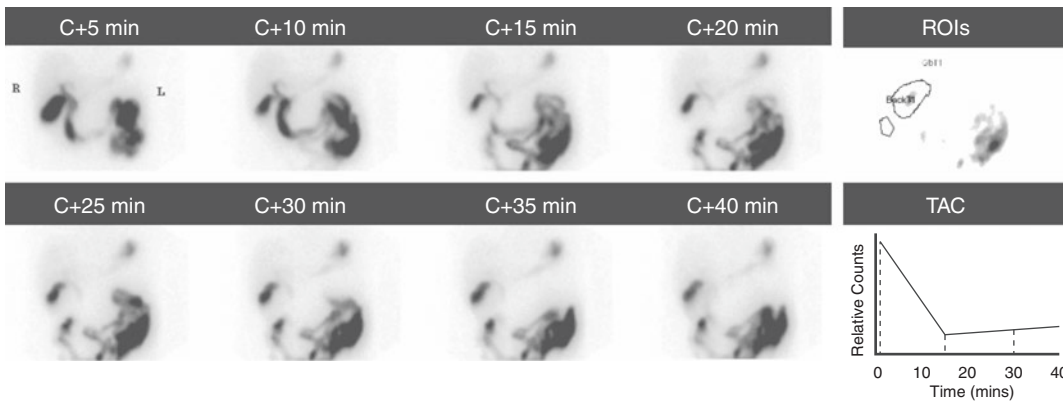

Fig. 7.5 Normal GB ejection fraction. Two micrograms of CCK-8 was administrated a 1 h by slow infusion and images were obtained over 40 min. There is prompt and excellent emptying of the GB. Time-activity curve (TAC) demonstrates an ejection fraction of 85%, which peaks at 12 min post-infusion

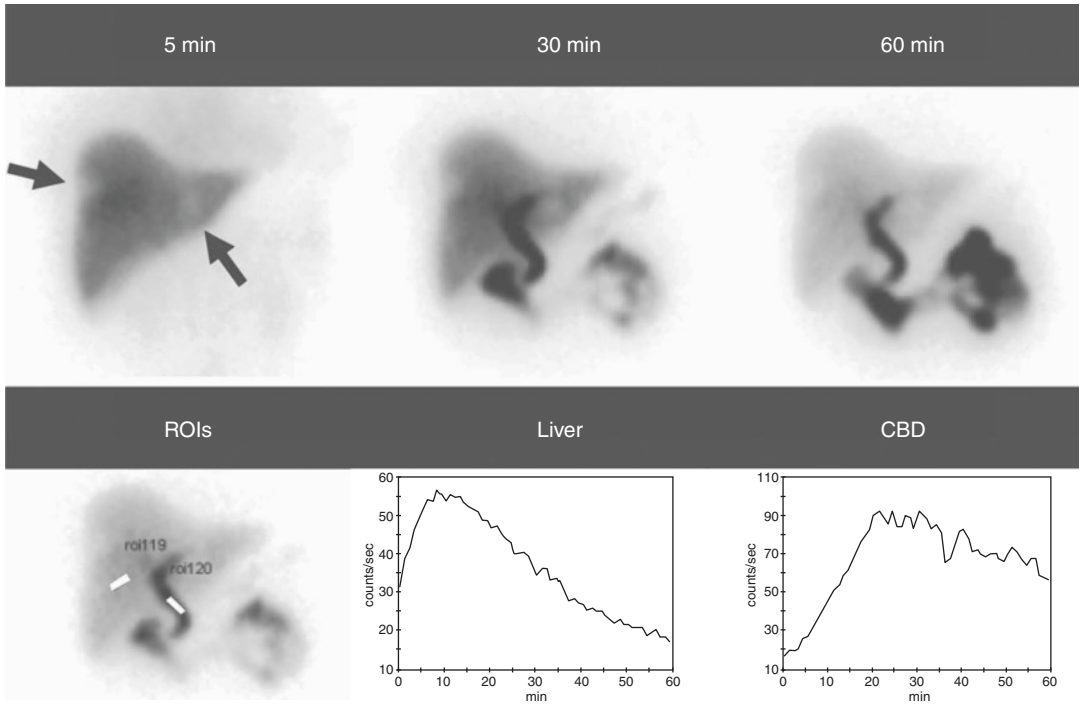

Fig. 7.6 A 28-year-old female with recurrent right-sided abdominal pain following cholecystectomy. Representative images at 5, 30, and 60 min are displayed (top row). Regions of interest (ROIs) were applied as per the method of Sostre et al. [20] in order to generate a quantitative score. TACs of indicated regions over the liver and common bile duct are displayed. For this patient, analysis does not support the diagnosis of sphincter of Oddi dysfunction. Incidentally noted are focal detects within the liver parenchyma due to two known hemangiomas (arrows)

7.2.3.4 Postoperative and Post-traumatic Patients

Because of the ability to track bile flow, biliary scintigraphy is effective in monitoring extravasation of bile following surgery [21, 22] or trauma [23]. Biliary scintigraphy is therefore used in symptomatic post-laparoscopic cholecystectomy patients, where reduced surgical exposure may lead to complications such as retained stones, transection, or ligation of the CBD [24] (Fig. 7.7). Scintigraphy is performed to visualize the expected flow of radiopharmaceutical from the liver into the bowel. Delayed images are helpful in identifying extravasated activity and can visualize loculated collections and free intraperitoneal leaks (Fig. 7.7), while decubitus views can be used to demonstrate free flow of intraperitoneal activity. In the current era, SPECT-CT is a powerful tool to enable precise anatomic localization of extravasated activity within a particular fluid collection.

Following trauma, collections may be observed on CT or US; however, their etiology may be unclear. Cholescintigraphy can help define a collection in relationship to biliary excretion in this context as well (Fig. 7.8). Flow of activity into a biloma is typically slow, and visualization may only appear on delayed images following gradual accumulation of radiopharmaceutical within the collection and maximal washout of activity from the normal liver [1]. Scintigraphy can be used to quantitate the degree of bile leak and thereby assess significance of injury [25] (Fig. 7.9). If the majority of bile flow progresses through the biliary tree into the duodenum, conservative management, rather than surgical repair, is usually attempted.

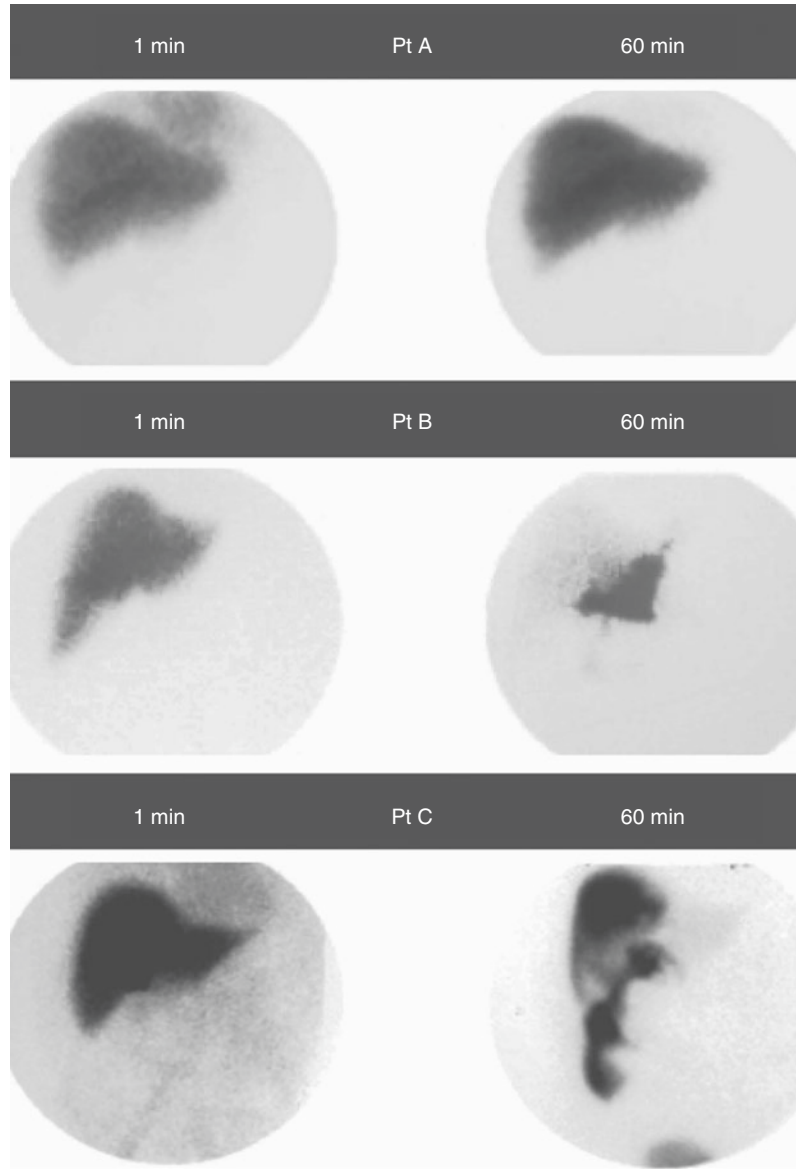

Fig. 7.7 Representative biliary scintigraphic images in three symptomatic post-laparoscopic cholecystectomy patients. Patient A is a 23-year-old female, 6 days post-procedure, who has increasing nausea, vomiting, and pain. A CBD obstructive pattern is noted. Patient B is a young female studied 10 days post-procedure. A relatively confined leak into the lesser sac is noted with negligible activity proceeding into the small bowel. Patient C also evidences a leak, which appears freely flowing down the right paracolic gutter (Reprinted from Zuckier and Freeman 2003 with permission)

7.2.3.5 Biliary Atresia

A specialized use of biliary scintigraphy is in differentiating biliary atresia from neonatal hepatitis. Infants are typically prepared by pretreatment with 5 mg/kg/day of phenobarbital, given orally in two divided doses, over a minimum of 3–5 days, designed to induce hepatic enzymes and maximize excretion of radiopharmaceutical [11, 26] (Table 7.2). For infants and children, 1.8 MBq/kg (0.05 mCi/kg) of radiopharmaceutical is typically administered with a minimum of 18.5 MBq (0.5 mCi) [6]. BRIDA is preferred to DISIDA due to its higher liver extraction. Imaging begins immediately postinjection and extends intermittently through several hours. If no bowel activity is observed, patients return for delayed imaging through 24 h. Any activity noted within the bowel or GB indicates patency

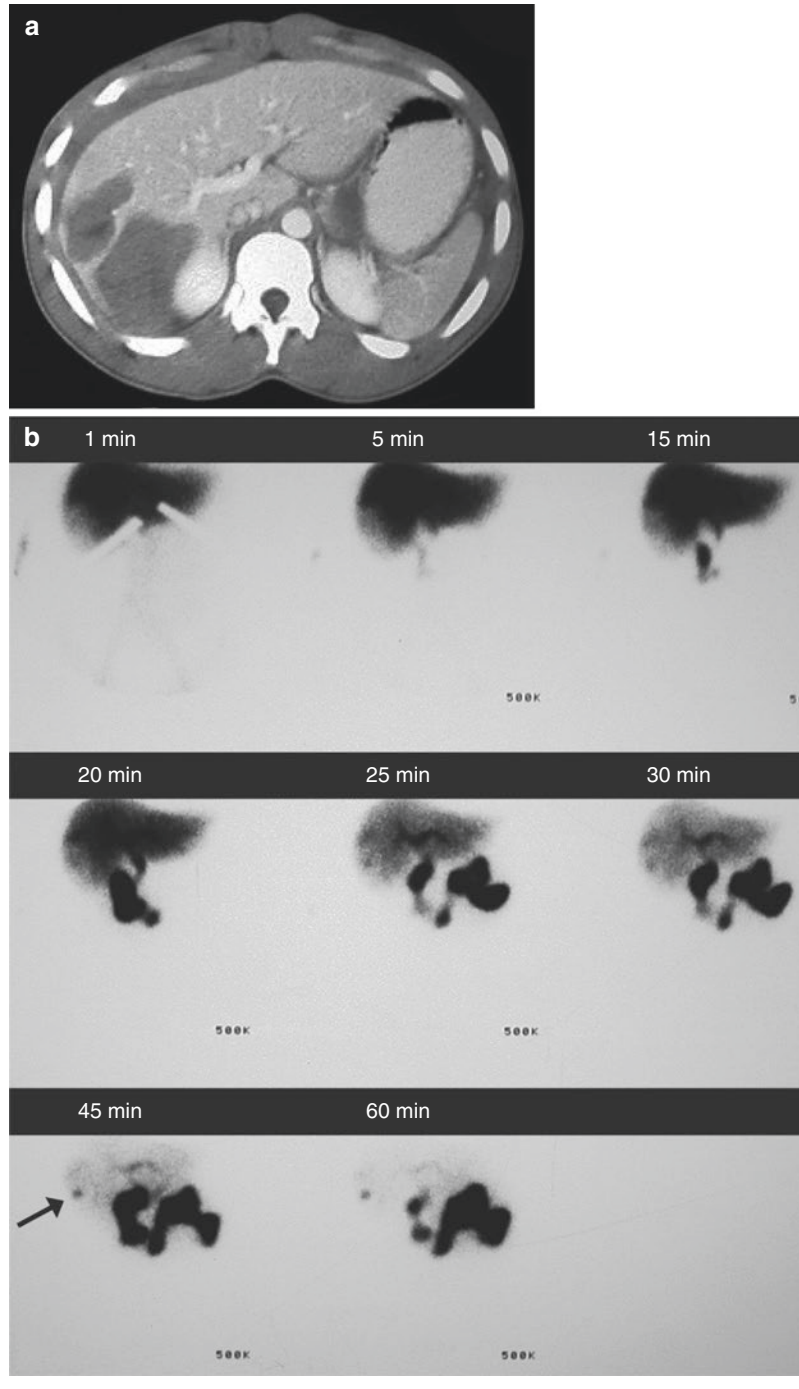

Fig. 7.8 Biloma following penetrating injury to the abdomen in an 18-year-old male who sustained a stab wound to his right flank. CT (**a**) demonstrates a large hemoperitoneum, laceration of the anterior and posterior segments of the right lobe of the liver, and a hematoma in Morrison's pouch. Biliary scintigraphy performed the following day (**b**) initially demonstrates presence of a photon-poor collection in the lateral aspect of the right lobe; however, over the hour course of imaging, a small focus of bile extravasation within the region of the collection is noted (arrow). The majority of the bile is excreted into the small bowel (Reprinted from Zuckier and Freeman 2003 with permission)

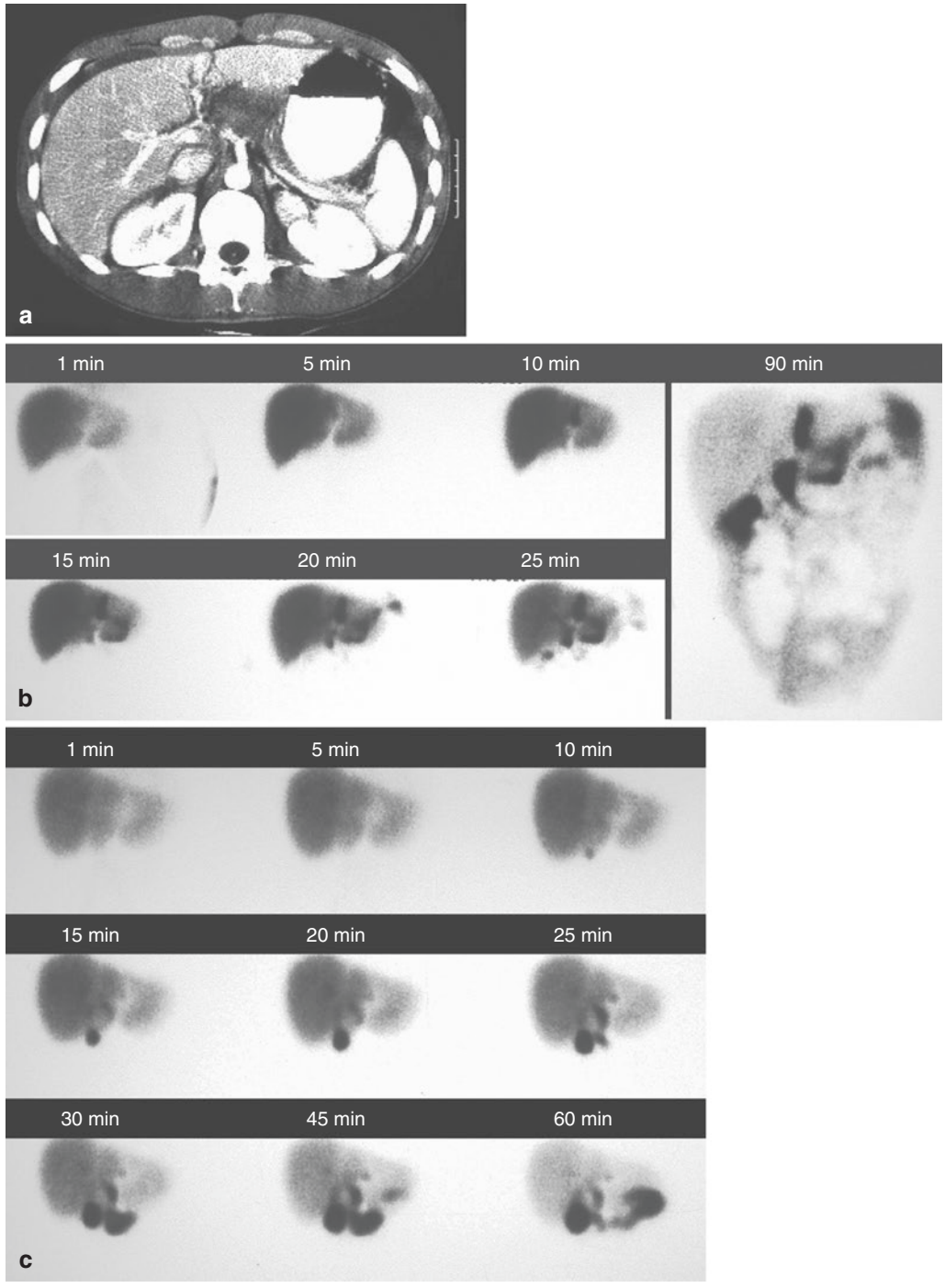

Fig. 7.9 Utility of biliary scintigraphy in evaluating traumatic injury to the liver and biliary structures in a 25-year-old male who was ejected from a car during a motor vehicle accident. A large liver laceration was noted on CT (**a**) with collection of fluid behind the left lobe of the liver. Initial biliary scintigraphy (**b**) demonstrates a large leak with spread of radiotracer throughout the peritoneal cavity by 90 min. Bowel loops are visualized as photon deficiencies. Follow-up scintigraphy performed after 5 days of conservative management (**c**) demonstrates near-complete resolution of the leak with progression of activity into the small bowel (Reprinted from Zuckier and Freeman 2003 with permission)

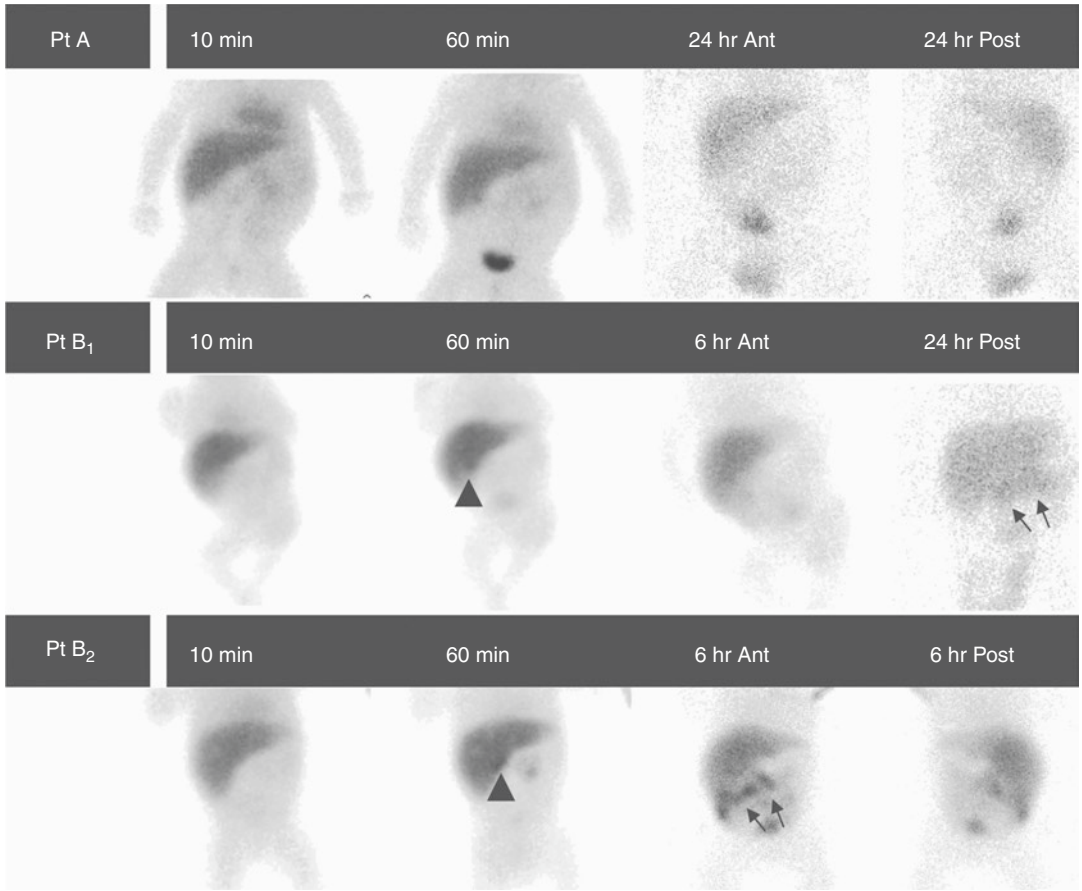

Fig. 7.10 Three separate studies performed on two infants to exclude biliary atresia. Patients were all administered phenobarbital prior to imaging in order to enhance excretion (see text and Table 7.2). Patient A: 4-month-old baby boy, delivered at a gestational age of 26 weeks, who presented with cholestatic jaundice. Persistent cardiac blood pool activity is noted up to 60 min of imaging, suggestive of hepatocellular dysfunction. Absence of gastrointestinal excretion of radiotracer in both early and 24-h delayed images is consistent with either biliary atresia or severe hepatocellular dysfunction. Activity within the kidneys and urinary system and diaper should not be confused with bowel excretion. Patient B is a 41-day-old baby girl who presented with increased bilirubin. Initial study (B_1) demonstrates relatively prompt uptake of radiotracer by the liver. The cardiac blood pool activity has cleared by 5 min. There is no evidence of radiotracer excretion into the GI system at the end of 1 h although the GB is faintly observed (arrowhead). Delayed images obtained at 6 h demonstrate vague activity into the intestine, while further delayed images obtained at 24 h confirm gastrointestinal excretion (arrows). Biliary atresia can therefore be excluded. Study was repeated 6 weeks thereafter (B_2). At this juncture, the GB is better visualized on the 60-min image (arrowhead), and bowel excretion is clearly noted on 6-h delayed images (arrows). These findings exclude biliary atresia

of the CBD and excludes the diagnosis of biliary atresia [27] (Fig. 7.10). When no bowel excretion is visualized, findings are ambiguous, as lack of excretion may be due to either severe neonatal hepatitis or biliary atresia [28]. In this instance, liver biopsy will be necessary to establish the diagnosis.

7.2.3.6 Characterization of Liver Masses

Biliary scintigraphy can contribute to the characterization of liver lesions (Table 7.1). Uptake of hepatobiliary radiopharmaceutical within a mass indicates presence of functioning hepatocytes and thereby excludes masses of non-hepatic origin. If

within a mass of hepatic origin the biliary radicals are not well developed, excretion of activity will be impaired, evidenced by slow washout and persistent activity on delayed imaging. For this reason, hepatocellular carcinoma (HCC) typically is best seen on delayed imaging several hours postinjection due to the combination of relatively reduced initial uptake by the tumor and slow washout and retention [29, 30]. In general, uptake within HCC correlates strongly with degree of tumor differentiation [31]. Slow washout of biliary radiopharmaceutical has also been noted in hepatic adenoma and FNH [32]. In cases where aspiration biopsy is inconclusive in differentiating well-differentiated HCCs from cirrhotic reactive changes, some have suggested utility in using delayed IDA imaging to differentiate well-differentiated HCCs, which may retain radiopharmaceutical, from cirrhotic reactive changes, which should not [29, 33, 34]. Unfortunately, no such distinction can be made scintigraphically between hepatic adenomas and HCCs, both of which may retain radiopharmaceutical.

7.3 Reticuloendothelial System Imaging of the Liver and Spleen

7.3.1 Radiopharmaceuticals

The distribution of the RE system is visualized following intravenous administration of radiolabeled colloids. Particles of SC range in size from 100 nm to approximately 1.0 μm. In the average patient, 80–90% of injected SC is phagocytized by the RE cells of the liver (Kupffer cells), 5–10% by the spleen, and the remainder by the bone marrow [35] (Fig. 7.11). A quantity of 111–222 MBq (3–6 mCi) of ^{99m}Tc-sulfur colloid (SC) is injected intravenously for imaging of the liver; when SPECT imaging is performed, the amount used is typically raised to 370 MBq (10 mCi) to provide a greater count rate [36, 37]. As a rule, smaller particles are preferentially taken up by marrow, while larger particles are phagocytized by the spleen. When more-targeted imaging of the spleen is necessary (see Sect. 7.3.3.3), imaging can be performed after injection of ^{99m}Tc-labeled heat-damaged RBCs, prepared by incubation of the labeled cells for 15 min in a water bath at 49–50 °C [36, 37]. Typically 37–222 MBQ (1–6 mCi) for planar imaging and 555–1100 MBq (15–20 mCi) for SPECT imaging is administered after cooling of the preparation to body temperature [37].

7.3.2 Methodology [36, 37]

Imaging of the liver and spleen commences approximately 10–20 min following SC injection. Flow studies obtained during injection are occasionally useful [37]. Planar views of the

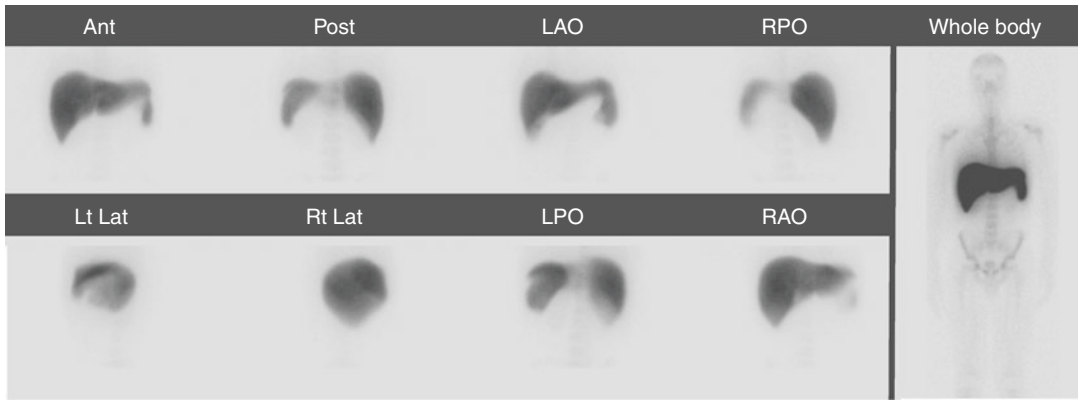

Fig. 7.11 Normal appearance of liver-spleen sulfur colloid scan in a 15-year-old boy. Standard planar views are shown in the left panel. Anterior whole-body view at increased intensity (right panel) illustrates the relative distribution of activity

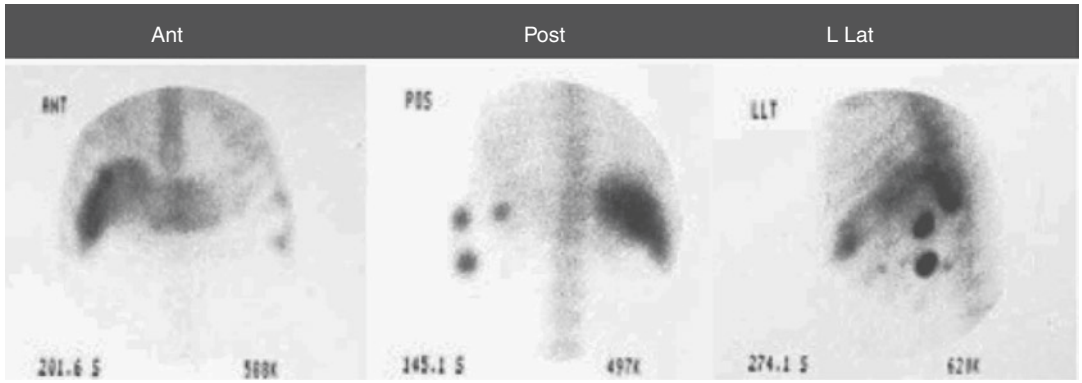

Fig. 7.12 Splenosis noted on a ^{99m}Tc-sulfur colloid study in a patient with cirrhosis and a remote history of abdominal trauma and splenectomy. In place of the spleen, three intense foci of activity are noted in the left upper quadrant of the abdomen, representing areas of functioning splenic tissue. Size and function of the spleen cannot be used to assess diffuse hepatic disease in the patient with splenectomy; however other signs may be observed. Uptake of colloid within the marrow is markedly increased and tertiary uptake in the lung is also noted. The liver appears small and there is separation of the lateral aspect of the liver from the rib margin (Helman's sign), suggesting ascites (Reprinted from Zuckier and Freeman 2003 with permission)

liver and spleen are taken in multiple obliquities (anterior, posterior, right lateral, right anterior oblique, right posterior oblique), or a tomographic SPECT image can be obtained. An image which includes a lead marker of standardized size placed on the costal margin is usually obtained in the planar technique. The left anterior oblique view, helpful in separating the left lobe of the liver from the spleen, and left posterior oblique and left lateral views are often added for imaging of the spleen. If ectopic splenic tissue is being evaluated, more extensive views of the entire abdomen, and possibly of the thorax as well [38], should be obtained (Fig. 7.12). On a large-field-of-view camera, the anterior image is usually acquired for approximately 500,000 to one million counts; other views are acquired for the same amount of time to facilitate comparison. SPECT imaging is especially helpful in resolving three-dimensional distributions of activity and in enabling comparison with findings on anatomic modalities, such as CT, US, and MRI. Current imaging on SPECT-CT cameras provides the optimum registration of nuclear medicine and CT images and has challenged the nuclear medicine physician to become proficient in the detection and diagnosis of liver incidentalomas [39].

7.3.3 Clinical Indications and Interpretation

Colloid studies of the liver are currently performed to assess diffuse hepatic disease and less frequently to evaluate focal processes within the liver. Colloid or ^{99m}Tc-labeled heat-damaged RBC splenic imaging is primarily performed to identify functional splenic tissue. These applications are discussed below.

7.3.3.1 Diffuse Parenchymal Disease of the Liver

Phagocytosis of particulate matter in the blood is an intrinsic function of the Kupffer cells of the liver [40]. The distribution of RE activity normally appears more intense in the liver than in the spleen, and marrow activity is generally only faintly appreciated. Variations in distribution of SC can therefore be used as a measure of hepatic function. In this sense, colloid scintigraphy yields information regarding physiologic function in addition to anatomy [41]. For evaluation of diffuse parenchymal liver disease, criteria of interpretation include hepatic size, splenic size, and the relative distribution of colloid between the various sites within the RES. Standardized technique is important as size of the colloid particles, and the prandial state of

the patient, affects quantitative parameters including the ratio of counts in the liver and spleen [42].

Features of the liver-spleen scan that correlate best with diffuse hepatocellular disease include moderate to severe inhomogeneous liver uptake, increased bone marrow uptake, and reversal of the normal liver-to-spleen uptake ratios [43] (Fig. 7.12). Colloid "shift" is not specific for hepatic dysfunction; factors including portal hypertension, hypersplenism, stimulation of the marrow as a response to chemotherapy, and malignant melanoma may also result in this finding. Splenomegaly is not a specific finding in hepatic disease, because other pathology, such as lymphoma, can alter splenic size [43, 44].

7.3.3.2 Focal Processes within the Liver

At one time, colloid scintigraphy had a role in identifying space-occupying lesions of the liver; today its use in identifying and characterizing focal processes within the liver is uncommon. Most true space-occupying processes within the liver, such as metastases and abscesses, are devoid of Kupffer cells, with resultant defects noted on SC imaging (Fig. 7.13). In contrast, processes that simulate space-occupying lesions on radiographic studies, but do not disturb Kupffer cell function, such as regenerating nodules or fatty change within the liver, retain SC uptake [45, 46]. Many investigators report sensitivity on the order of 80–85% for detecting liver metastases [47]; surface lesions less than 2 cm, and deep lesions less than 3–4 cm in diameter, may not be well visualized on planar scintigraphy due to spatial-resolution limitations of the gamma-camera [48]. At low disease prevalence, SPECT has been shown to offer only a marginal benefit over planar scintigraphy [49]. SPECT slightly improves the detection of small lesions, but may cause a concomitant decrease in specificity, as small normal structures, such as vessels or ducts, may become visible and simulate lesions [48]. Advent of SPECT-CT systems may obviate this confusion and improve tomographic colloid studies by combining physiology and anatomic detail.

Primary masses originating within the liver include HCC, focal nodular hyperplasia (FNH),

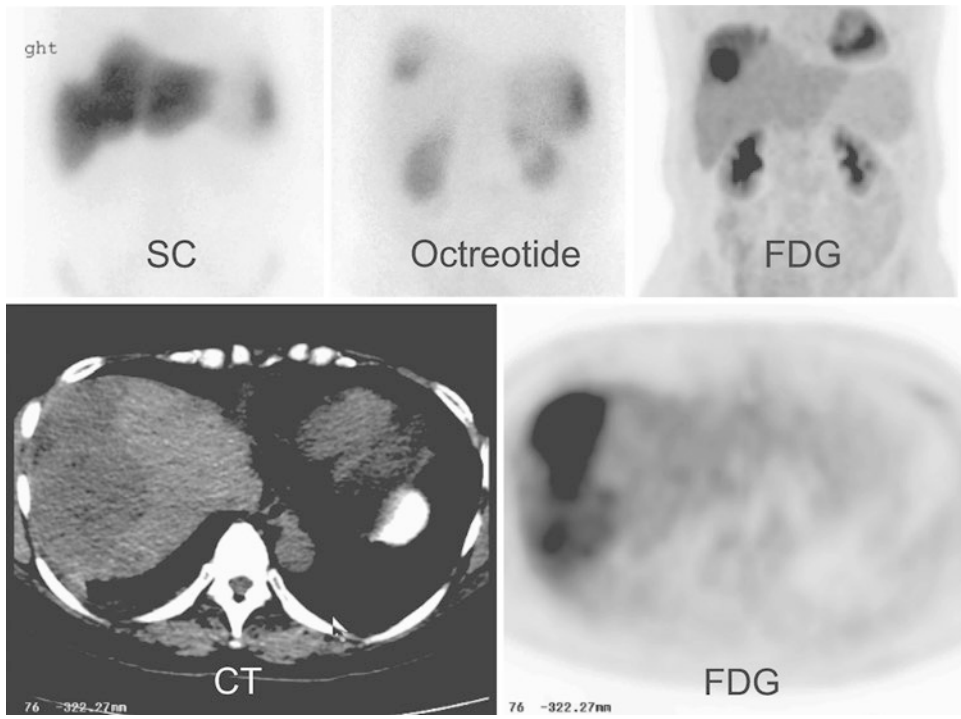

Fig. 7.13 A 48-year-old female with history of pancreatic carcinoid tumor metastatic to the liver. Anterior ^{99m}Tc-sulfur colloid image demonstrates a defect in the superior aspect of the liver. Focal uptake is noted on ^{111}In-octreotide anterior planar image and ^{18}F-FDG anterior MIP image, consistent with metastatic carcinoid tumor. On the lower panels, transaxial PET-CT images illustrate FDG uptake corresponding to a low-density liver metastasis

and hepatic adenoma. HCC is devoid of uptake on SC studies. In FNH, lesions have variable degrees of Kupffer cell function, and consequently variable colloid uptake has been described in these lesions ranging from decreased (in 30% of lesions) to normal (30%), to supranormal (30%), and even to intense (10%) [50]. Recent scintigraphic and pathologic literature has also documented possible presence of Kupffer cells in hepatic adenomas [51, 52], with moderate uptake in up to one-quarter of the patients studied. Masses with uptake above normal are believed to be relatively pathognomonic for FNH, Table 7.3 (Fig. 7.14).

In addition to FNH, several vascular derangements may lead to focal regions of increased SC uptake within the liver (Table 7.4). In superior

Table 7.3 Variable Colloid and IDA uptake patterns as a function of hepatic space-occupying lesions[a]

Space-occupying lesion	^{99m}Tc-sulfur colloid	^{99m}Tc-HIDA
Hepatoma	Cold (↓↓)	Cold (↓↓). May show slow uptake without washout
Hepatic adenoma	Variable reduced (↓↓ to ↓)	Uptake with slow washout
Focal nodular hyperplasia	Variable (↓↓ to ↑↑)	Uptake with slow washout
Liver metastases	Cold (↓↓)	Cold (↓↓)

↓ mildly decreased, ↓↓ markedly decreased, ↑↑ markedly increased

[a]After Drane [32]

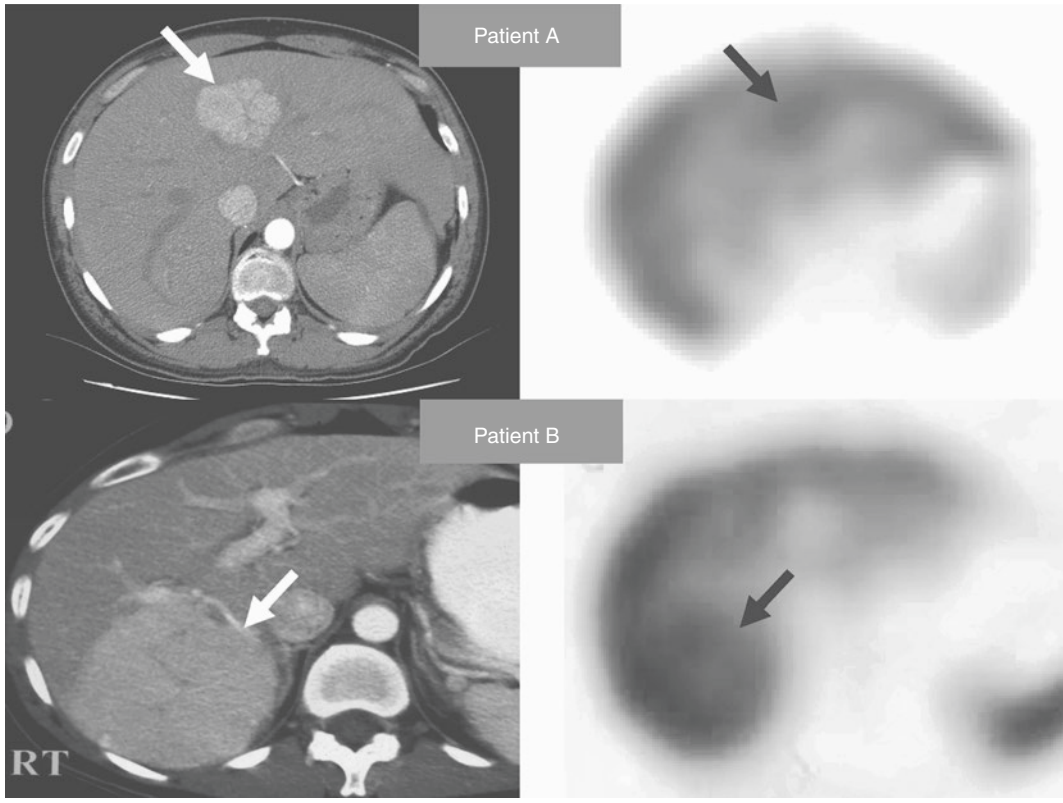

Fig. 7.14 Two examples of relatively intense uptake of SC in FNH. On non-AC corrected SPECT imaging, the center of the liver normally appears less intense than the periphery due to the effect of photon attenuation. Patient A is a 38-year-old woman with abdominal discomfort noted to have an enhancing lesion within the right lobe of the liver (arrow) on CT scan. Tomographic image from a liver-spleen colloid scan shows an area of increased colloid uptake relative to the surrounding liver, pathognomonic of FNH. Patient B is a 42-year-old woman with a liver mass incidentally detected on sonography. An area of relatively intense SC uptake is seen corresponding to the enhancing mass seen on arterial phase CT (arrow)

vena cava (SVC) obstruction, a venous injection of SC into the upper extremities must bypass the occluded SVC and reach the heart via porto-systemic collaterals, typically through the internal mammary vein that connects to the paraumbilical and left portal vein [53, 54]. Adjacent regions of the liver, specifically the medial segment of the left lobe, receive relatively enriched amounts of colloid and consequently appear intense on subsequent imaging (Fig. 7.15). In obstruction of the inferior vena cava (IVC), a similar finding has been noted following injection of radiotracer via the lower extremities though in this case injection via the upper extremities will result in a normal distribution of activity [55].

Table 7.4 Vascular causes of relative "hot spots" in the liver

Disorder	Region	Mechanism
Budd-Chiari syndrome	Caudate lobe	Direct drainage by accessory vein
SVC or IVC obstruction	Quadrate lobe	Collateral pathway to the left portal vein
Ethanol abuse	Left lobe	"Streamlining" of toxins to the right lobe

In Budd-Chiari syndrome, hepatic venous drainage into the SVC is obstructed, thereby impairing overall liver function. In contrast, the liver parenchyma in the region of the caudate lobe often drains directly into the adjacent SVC via accessory veins. This segment thereby exhibits relatively intact uptake of colloid in comparison

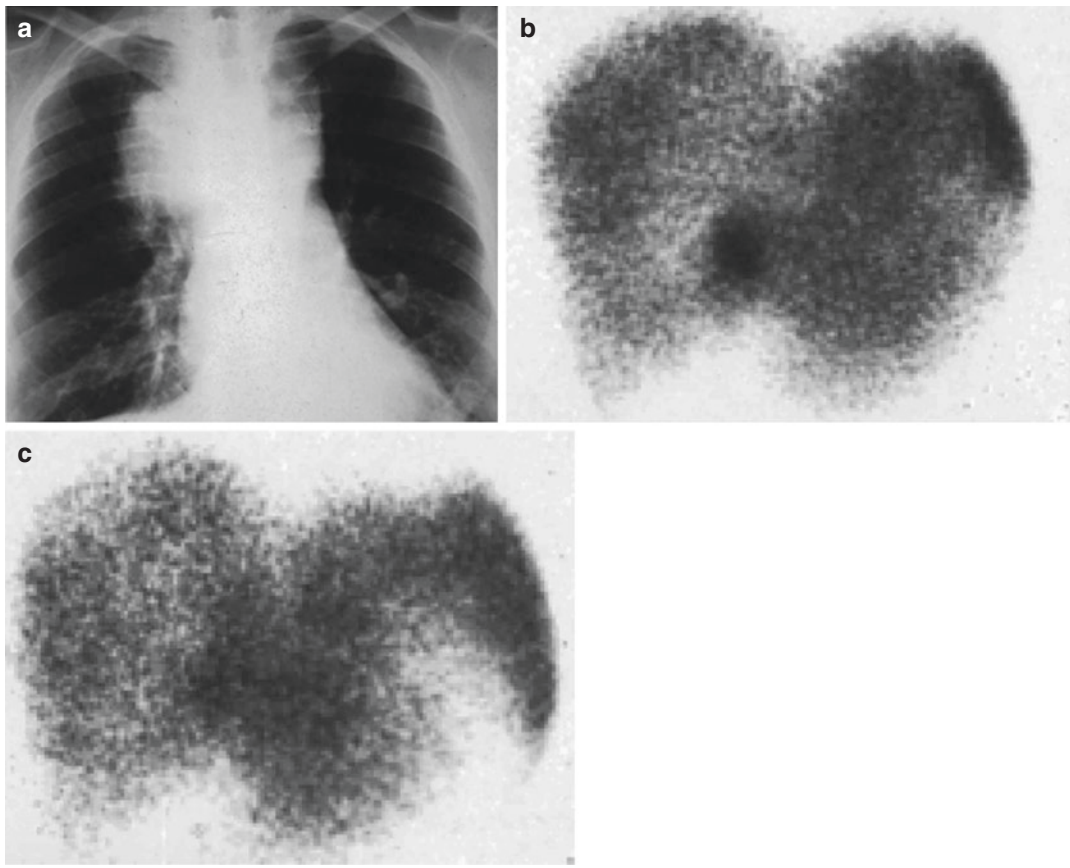

Fig. 7.15 Adult male with obstruction of the SVC caused by mediastinal malignancy (**a**). Anterior view from liver-spleen colloid scan (**b**) shows presence of a hot region in the medial aspect of the right lobe ("quadrate lobe"), due to collateralization of blood flow through the umbilical vein. Following radiotherapy to the mediastinum, the area of increased hepatic uptake resolves (**c**)

to the remainder of the affected liver, a finding coined the "bullseye" sign [56].

An additional cause of relatively increased uptake within the liver may be seen in alcoholic liver disease, which preferentially affects the right lobe of the liver resulting in an "intrahepatic colloid shift" from the severely affected right lobe to the relatively preserved left lobe. This phenomenon is believed to be due to asymmetric "streamlining" of toxic portal venous blood within the lobes of the liver [57].

7.3.3.3 Splenic Imaging

Utility of colloid imaging of the spleen derives from a relatively high degree of tissue specificity based on the functional nature of the examination. Because larger particles preferentially localize in the spleen, denatured RBCs are superior to SC for splenic imaging [58, 59], although this more-complicated procedure is currently only selectively employed.

Splenic imaging may be performed in children to rule out congenital asplenia or polysplenia. SPECT imaging is especially valuable for this purpose because of the ability to resolve splenic uptake adjacent to the liver as distinct from the liver itself [60]. Other indications for splenic imaging include confirming presence of functional splenic tissue in cases of splenic autotransplantation following splenic trauma (Fig. 7.12) or absence of such tissue in patients who have been treated previously with splenectomy for conditions such as idiopathic thrombocytopenic purpura (ITP) [59]. Splenic imaging can also be performed in order to characterize incidentally noted abdominal masses, which may represent accessory spleens or splenic tissue rather than malignant deposits (Fig. 7.16).

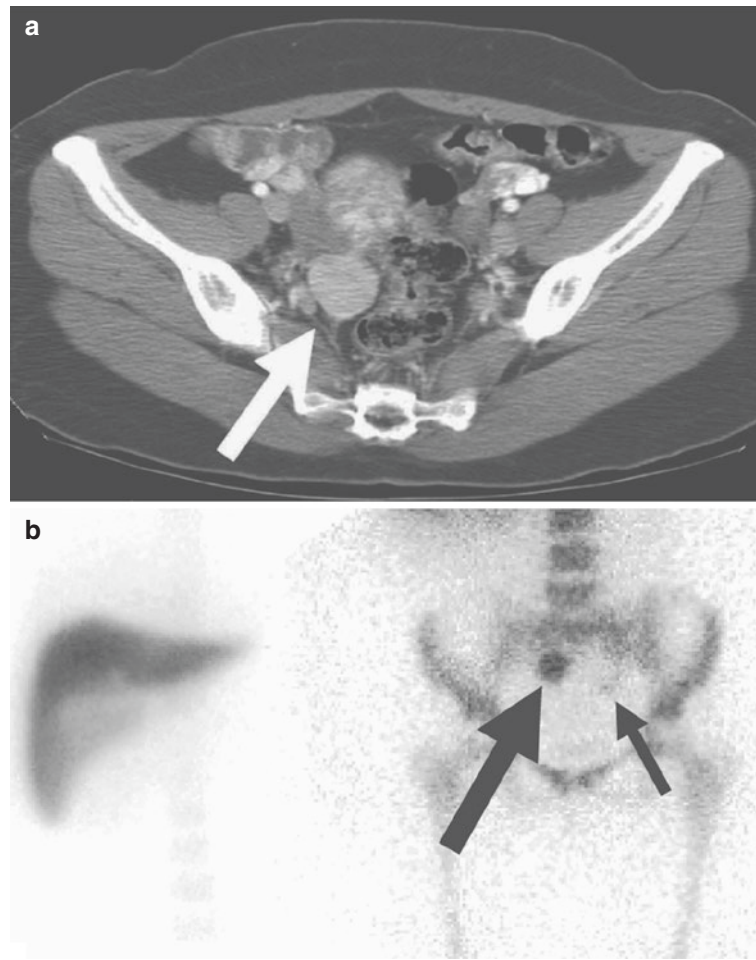

Fig. 7.16 Contrast-enhanced CT scan (**a**) in this 36-year-old Hispanic female demonstrates several enhancing masses within the abdomen and pelvis (one such pelvic mass is illustrated by arrow). History was significant for a motor vehicle accident several years earlier with probable splenectomy. Colloid study demonstrates absence of orthotopic spleen (**b**). When viewed at increased intensity, a prominent focus of colloid accumulation is noted anterior to the right SI joint corresponding to the region of the enhancing mass (large arrow) with a smaller focus noted inferior to the left SI joint (small arrow), both of which are caused by splenosis

7.4 Hemangioma Imaging

The most common benign lesion of the liver is hemangioma, occurring in up to 7% of the population and therefore representing a frequent incidental finding in the course of imaging of the abdomen [61]. Hemangiomas are typically less than 3 cm in diameter; when larger than 4 cm, they bear the designation "giant" [62]. As a rule, hemangiomas do not require any medical intervention or treatment, and a noninvasive and specific means of characterizing these lesions would serve to obviate further concern. Imaging of the liver with ^{99m}Tc-labeled RBCs fulfills this role.

7.4.1 Radiopharmaceuticals

For identification of hemangioma, 740–925 MBq (20–25 mCi) of ^{99m}Tc-RBCs is used [36, 37], optimally labeled by the in vitro method. Methods of RBC labeling are common to other scintigraphic applications, such as GI bleeding studies, and are discussed elsewhere in this book.

7.4.2 Methodology [36, 37]

Prior to hemangioma imaging, it is important to identify location of the suspect lesion, most commonly by reference to the previously obtained CT, US, or MRI study. Where no prior images are available for consultation, a low-dose SC study can be performed immediately preceding RBC imaging to define the defect; however, this procedure is usually unnecessary where other cross-sectional images are available for consultation. Generally, imaging consists of three phases: arterial perfusion (flow), immediate blood pool, and delayed blood pool [63]. Arterial perfusion imaging, typically obtained at one to three frames per second during injection of the labeled RBCs, reveals useful information about regional distribution of hepatic arterial blood flow and should be performed in the view best-predicted to portray the lesion while avoiding overlap with normal vascular structures. Care should be exercised so as to not hemolyze the blood with a rapid injection through a narrow catheter. Immediate blood pool images are then acquired for 1–2 million counts each, in this optimal projection as well as in standard anterior, posterior, and right lateral views. Delayed blood pool images, designed to portray the maximal washin of RBCs into the hemangioma, are acquired approximately 1–2 h following injection in similar projections to the immediate blood pool images. SPECT (possibly in combination with CT) will often be necessary to visualize small lesions, especially when deep within the liver parenchyma or not detected on planar views [64], and is useful for comparison to other cross-sectional imaging modalities.

7.4.3 Clinical Indications and Interpretation

Classic findings in hemangioma are absent visualization during arterial perfusion imaging, while on blood pool imaging, the lesion becomes more intense than surrounding normal liver, a phenomenon termed the "perfusion-blood pool mismatch" [52] (Fig. 7.17). Activity greater than adjacent liver is observed on the 2- to 3-h delayed image but may even be evident on the immediate blood pool images.

Overall imaging accuracy for detecting hemangiomas is reported to be 90%, especially if SPECT is used for smaller lesions. Sensitivity for characterizing hemangiomas greater than 2–3 cm in diameter is high; smaller lesions can be best detected when peripheral and SPECT is performed [64, 65]. In giant cavernous hemangiomas, RBC SPECT has been shown to be useful in differentiation from other large liver masses and is superior to US [66]. False-negative results have been rarely seen in hemangiomas with extensive fibrosis and thrombosis [67] or when attempting to visualize lesions below the effective resolution. False-positive studies demonstrating increased blood pool have been rarely described in patients with hemangiosarcoma [68] and very rarely in HCC. In a meta-analysis of 365 patients with 254 hemangiomas [63], the unusual combination of early flow and delayed intense filling was present in 16 lesions (4.4%). Twelve of these cases were determined to be hemangioma,

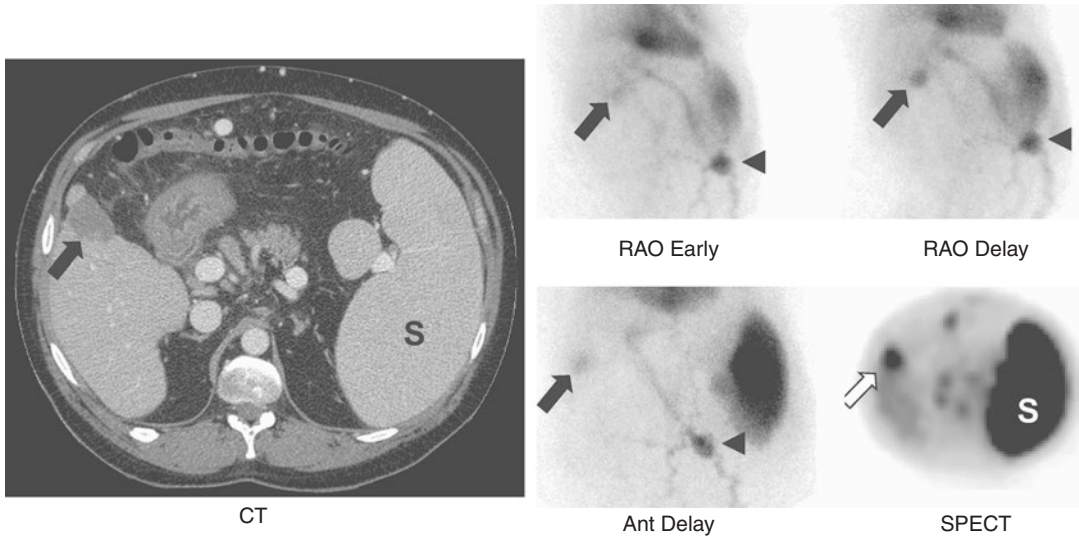

Fig. 7.17 A 50-year-old male with hepatitis C and alcoholic cirrhosis. CT scan of the abdomen (left panel) suggests hemangioma of the liver (arrow). Multiple venous collaterals are noted throughout the abdomen. Images from RBC hemangioma study (right panels) demonstrate presence of intense blood pool in the region of the lesion, increasing between the early and delayed images. The spleen (*S*) is enlarged and multiple venous anastomoses over the abdomen are noted (arrowhead, *caput medusae*)

while four were diagnosed as HCC. In an effort to increase specificity, these authors recommended restricting the diagnosis of hemangioma to lesions that do not evidence increased arterial perfusion, even though sensitivity will be slightly reduced. When increased arterial flow is present, as in the 4.4% of examinations in their meta-analysis, additional diagnostic studies and biopsy are then needed to make a definitive diagnosis.

7.5 Other Ancillary Techniques

7.5.1 ^{18}F-Fluorodeoxyglucose PET

^{18}F-Fluorodeoxyglucose (FDG) PET has become a mainstay of oncologic imaging [69], discussed elsewhere in this text. It is therefore not surprising that this modality has been successfully used in evaluating tumors of the liver and GI tract (Fig. 7.13). Liver tissue normally exhibits moderate FDG uptake with standardized uptake values (SUVs) typically on the order of 2.0. Increased FDG uptake in tumor cells has been shown to be due to increased expression of glucose transporter (GLUT) molecules on the cell surface, increased activity of hexokinase, and reduced levels of glucose-6-phosphatase [70].

Uptake of FDG is not restricted to malignancy, and various inflammatory and infectious states can lead to increased FDG uptake, by virtue of the collection of cells and organisms that utilize glucose and its analogs. This can include tuberculous [71], mycotic, and pyogenic abscesses.

7.5.2 Hepatic Arterial Perfusion Scintigraphy [37, 72]

Hepatic arterial perfusion scintigraphy (HAPS) was initially developed and is still used as a means of confirming proper placement of hepatic artery chemotherapy infusion catheters prior to delivery of arterial chemotherapy to intrahepatic tumors [73, 74]. A quantity of 37–185 MBq (1–5 mCi) of ^{99m}Tc-macroaggregated albumin (MAA), particle size 10–90 μm, is injected through an infusion catheter placed in the hepatic artery, resulting in trapping of radiopharmaceutical within the

downstream perfused capillary bed [37]. The rate of injection should be less than 1 ml/min to avoid creating artifactual perfusion patterns and should optimally be similar to that of the proposed therapeutic agent. The distribution of activity is subsequently imaged using planar, SPECT, or SPECT-CT scintigraphy, including views of the lungs to identify intrahepatic arteriovenous fistulas. If SPECT-CT is not available, comparison to imaging of the liver following injection of colloid may be helpful [37]. This technique has been adopted as a sensitive means of detecting intrahepatic metastases based on the differences in perfusion of normal liver parenchyma, largely via the portal vein, versus intrahepatic metastases, via the hepatic artery. Metastatic lesions as small as 0.5–1.0 cm in size may be detected as "hot spots" [75]. Small lesions have been identified that were not seen by CT or CT arterial portography and which could only be confirmed at blind resection or biopsy [76]. While effective, HAPS is not commonly performed for detection of intrahepatic malignancy due to the invasiveness of placing an injection catheter into the hepatic artery.

Based on similar physiologic principles, treatment with ^{90}Y-containing microspheres has been introduced as a means of delivering localized radiation to sites of hepatocellular carcinoma and metastatic lesions [72, 77, 78]. Prior to treatment, hepatopulmonary shunting secondary to tumor-related pathologic arteriovenous channels, as well as reflux toward the gastrointestinal region, should be evaluated at scintigraphy following injection of 5–6 mCi (185–222 MBq) of ^{99m}Tc-labeled MAA as a microsphere surrogate into the hepatic arterial territory (see also Chap. 38) [79–81].

7.5.3 ^{133}Xenon Gas

Though not commonly performed today, radioactive xenon has historically been used to identify focal fatty changes in the liver, based on retention of the radioactive gas within the liver on delayed washout studies [82–84]. When the liver exhibits only a moderate degree of hepatic steatosis, a normal SC examination appears to be a more reliable [45] and available scintigraphic means of excluding pathology.

7.5.4 ^{123}I- and ^{131}I-Metaiodobenzylguanadine

^{123}I- and ^{131}I-metaiodobenzylguanadine (MIBG) is used in the imaging of pheochromocytomas, paragangliomas, neuroblastoma, carcinoid, and medullary thyroid tumors and can be helpful in evaluating lesions metastatic to the liver [85–87]. MIBG is a guanidine derivative, structurally similar to norepinephrine, that concentrates within secretory granules of catecholamine-producing cells. Correlation with anatomic imaging is important in achieving accuracy [88].

The ^{123}I-labeled analog has superior imaging and dosimetry characteristics and is preferred if available. Some authors have reported relatively higher concentration of MIBG in normal parenchyma of the left lobe of the liver as compared to the right, possibly due to a greater presence of catecholamines and a higher sympathetic nerve density [89]. MIBG imaging may be useful in selecting patients slated for therapy with therapeutic amounts of ^{131}I-MIBG (s. also Chaps. 13 and 35) [90].

7.5.5 ^{111}In-Octreotide (Octreoscan) and ^{68}Ga-DOTATATE

^{111}In-octreotide represents a receptor binding radiopharmaceutical that is used in the staging of various endocrinologic tumors and can detect presence of liver metastases (Figs. 7.13, 7.18). This ^{111}In-labeled somatostatin analog binds to the sstr2 receptor that is present on the extracellular membrane of numerous neuroendocrine tumor (NET) types [70]. Overall, reported sensitivity of ^{111}In-octreotide is 80–90% for gastrinomas, 70% for carcinoids, 40% for insulinomas, and 30% for glucagonoma [91]. Somatostatin receptor scintigraphy has been shown to be superior to FDG PET for diagnosing and staging carcinoid tumors; the latter should be reserved for patients with negative results on octreotide

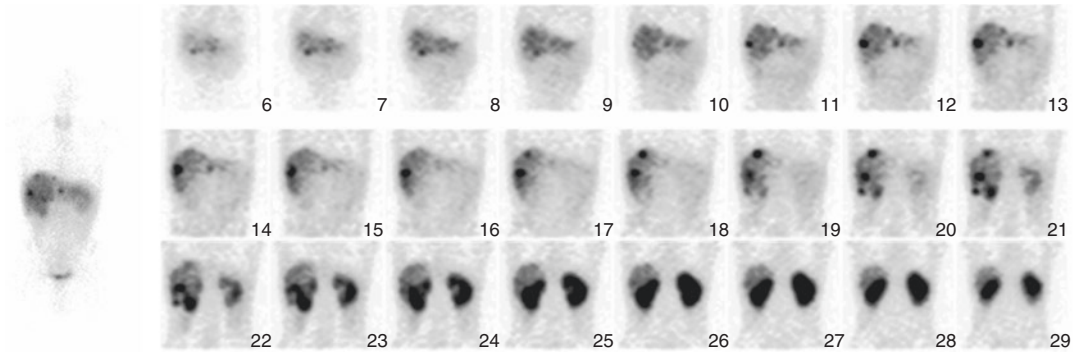

Fig. 7.18 A 42-year-old male with history of carcinoid tumor. Whole-body image (left panel) and sequential coronal SPECT images (right panel) were obtained 24 h following injection of ^{111}In-octreotide. Numerous foci of radiopharmaceutical uptake are noted which stud the liver. Physiologic excretion of octreotide is noted on posterior tomographic images through the kidneys (*frames 22–29*)

scintigraphy [92]. In the current era, analogous PET tracers have enjoyed considerable success in the imaging of NET-type tumors, especially ^{68}Ga-DOTATATE [93]. The uncinate process of the pancreas may physiologically exhibit increased radiopharmaceutical uptake; this pattern should be recognized as a normal variant [93, 94]. These applications will be discussed in Chaps. 13 and 34.

7.5.6 ^{67}Ga-Citrate

Since the 1970s, ^{67}Ga-citrate has been known to accumulate in both malignant and infectious processes that affect the liver [95]. More recently, the mechanism of localization of ^{67}Ga-citrate in tumors has been understood to be receptor based, reflecting increased presence of transferrin receptors to which circulating ^{67}Ga-transferrin complexes bind [96]. Comparison to SC imaging is recommended [48], as a gallium-avid tumor may appear isointense to normal liver and would therefore be difficult to diagnose on gallium scan alone though it would be readily identifiable when compared to the defect on a SC or other anatomic studies.

Approximately 90–95% of HCCs are reported to have ^{67}Ga-citrate uptake, and this radiopharmaceutical has historically served an important ancillary role in making this diagnosis [95, 97, 98] (Fig. 7.19) though today gallium imaging is not usually employed in this diagnosis. In addition to HCC, other tumor types that are frequently ^{67}Ga-citrate avid include lymphoma and metastases from lung carcinoma, melanoma, colorectal carcinoma, sarcoma, and testicular neoplasms. A variety of abscesses concentrate gallium citrate, and this application is discussed elsewhere in this book under the topic of infection imaging (Chap. 16).

7.6 Summary and Future Developments

Scintigraphic imaging retains a role in the functional and noninvasive evaluation of the solid GI tract. In the near future, the area of greatest growth which will likely impact on this modality is the continued development of novel PET radiopharmaceuticals that target those tumors presently not well localized by the currently available radiopharmaceutical ^{18}F-FDG [99]. Increasing experience and knowledge will also lead to consolidation of radionuclide studies into diagnostic and treatment algorithms. Through fusion of scintigraphic images with CT, hybrid imaging seeks to combine the functional strength of scintigraphic imaging with the superior resolution of anatomic radiologic modalities.

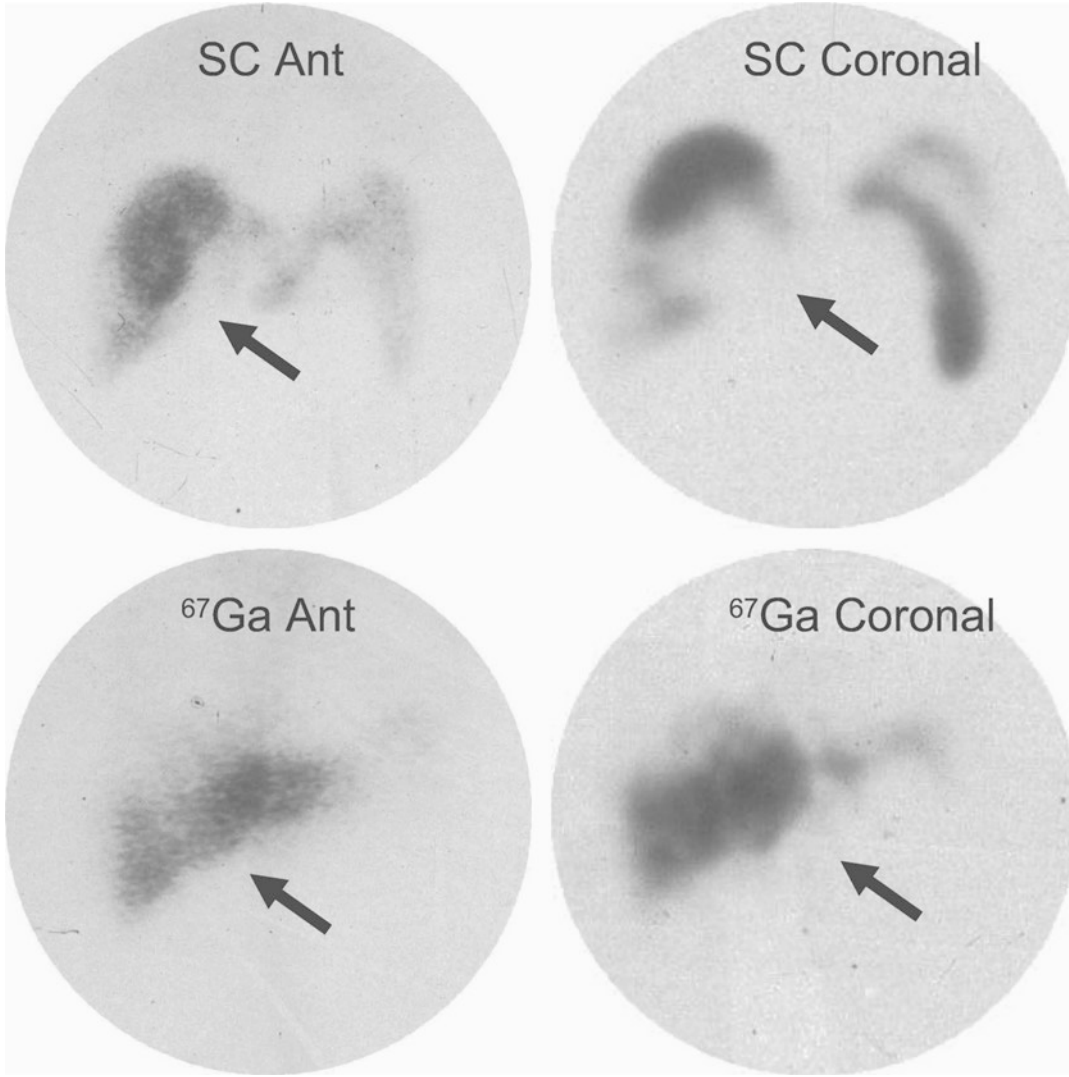

Fig. 7.19 A 63-year-old alcoholic patient with markedly elevated alpha-fetal protein. Sulfur colloid images (upper panels) demonstrate heterogeneous defects within the liver, especially inferiorly (arrows). The spleen appears enlarged on the coronal SPECT image (right upper panel). ^{67}Ga-gallium citrate images (lower panels) demonstrate gallium-avid HCC replacing hepatic tissue in region of defects noted on the colloid study (Reprinted from Middleton et al. 1994 with permission)

References

1. Zuckier LS, Freeman LM. Selective role of nuclear medicine in evaluating the acute abdomen. Radiol Clin North Am. 2003;41:1275–88.
2. Wistow BW, Subramanian G, Heertum RL, Henderson RW, Gagne GM, Hall RC, McAfee JG. An evaluation of 99mTc-labeled hepatobiliary agents. J Nucl Med. 1977;18:455–61.
3. Saremi F, Jadvar H, Siegel ME. Pharmacologic interventions in nuclear radiology: indications, imaging protocols, and clinical results. Radiographics. 2002;22:477–90.
4. Ziessman HA. Interventions used with cholescintigraphy for the diagnosis of hepatobiliary disease. Semin Nucl Med. 2009;39:174–85.
5. Gerard PS, Brown RKJ, Parisi MT, Tulchinsky M, Biyyam DR, Servaes S, Treves ST. ACR–SPR practice parameter for the performance of hepatobiliary scintigraphy. ACR–SPR. 2017;2017:1–8.

6. Tulchinsky M, Ciak BW, Delbeke D, Hilson A, Holes-Lewis KA, Stabin MG, Ziessman HA. SNM practice guideline for hepatobiliary scintigraphy 4.0. J Nucl Med Technol. 2010;38:210–8.
7. Kim CK, Palestro CJ, Solomon RW, Molinari DS, Lee SO, Goldsmith SJ. Delayed biliary-to-bowel transit in cholescintigraphy after cholecystokinin treatment. Radiology. 1990;176:553–6.
8. Weissmann HS, Frank MS, Bernstein LH, Freeman LM. Rapid and accurate diagnosis of acute cholecystitis with 99mTc-HIDA cholescintigraphy. AJR. 1979;132:523–8.
9. Weissmann HS, Berkowitz D, Fox MS, Gliedman ML, Rosenblatt R, Sugarman LA, Freeman LM. The role of technetium-99m iminodiacetic acid (IDA) cholescintigraphy in acute acalculous cholecystitis. Radiology. 1983;146:177–80.
10. Kiewiet JJ, Leeuwenburgh MM, Bipat S, Bossuyt PM, Stoker J, Boermeester MA. A systematic review and meta-analysis of diagnostic performance of imaging in acute cholecystitis. Radiology. 2012;264:708–20.
11. Fink-Bennett D, Balon H, Robbins T, Tsai D. Morphine-augmented cholescintigraphy: its efficacy in detecting acute cholecystitis. J Nucl Med. 1991;32:1231–3.
12. Kim CK, Juweid M, Woda A, Rothstein RD, Alavi A. Hepatobiliary scintigraphy: morphine-augmented versus delayed imaging in patients with suspected acute cholecystitis. J Nucl Med. 1993;34:506–9.
13. Meekin GK, Ziessman HA, Klappenbach RS. Prognostic value and pathophysiologic significance of the rim sign in cholescintigraphy. J Nucl Med. 1987;28:1679–82.
14. Smith R, Rosen JM, Gallo LN, Alderson PO. Pericholecystic hepatic activity in cholescintigraphy. Radiology. 1985;156:797–800.
15. DiBaise JK, Richmond BK, Ziessman HA, Everson GT, Fanelli RD, Maurer AH, Ouyang A, Shamamian P, Simons RJ, Wall LA, Weida TJ, Tulchinsky M. Cholecystokinin-cholescintigraphy in adults: consensus recommendations of an interdisciplinary panel. Clin Nucl Med. 2012;37:63–70.
16. Ziessman HA, Tulchinsky M, Lavely WC, Gaughan JP, Allen TW, Maru A, Parkman HP, Maurer AH. Sincalide-stimulated cholescintigraphy: a multicenter investigation to determine optimal infusion methodology and gallbladder ejection fraction normal values. J Nucl Med. 2010;51:277–81.
17. Krishnamurthy GT, Brown PH. Comparison of fatty meal and intravenous cholecystokinin infusion for gallbladder ejection fraction. J Nucl Med. 2002;43:1603–10.
18. Ziessman HA, Jones DA, Muenz LR, Agarval AK. Cholecystokinin cholescintigraphy: methodology and normal values using a lactose-free fatty-meal food supplement. J Nucl Med. 2003;44:1263–6.
19. Ziessman HA. Cholecystokinin cholescintigraphy: victim of its own success? J Nucl Med. 1999;40:2038–42.
20. Sostre S, Kalloo AN, Spiegler EJ, Camargo EE, Wagner HN Jr. A noninvasive test of sphincter of Oddi dysfunction in postcholecystectomy patients: the scintigraphic score. J Nucl Med. 1992;33:1216–22.
21. Matesan M, Bermo M, Cruite I, Shih CH, Elojeimy S, Behnia F, Lewis D, Vesselle H. Biliary leak in the postsurgical abdomen: a primer to HIDA scan interpretation. Semin Nucl Med. 2017;47:618–29.
22. Trerotola SO, Savader SJ, Lund GB, Venbrux AC, Sostre S, Lillemoe KD, Cameron JL, Osterman FA Jr. Biliary tract complications following laparoscopic cholecystectomy: imaging and intervention. Radiology. 1992;184:195–200.
23. Zeman RK, Lee CH, Stahl R, Viscomi GN, Baker C, Cahow CE, Dobbins J, Neumann R, Burrell MI. Strategy for the use of biliary scintigraphy in noniatrogenic biliary trauma. Radiology. 1984;151:771–7.
24. Estrada WN, Zanzi I, Ward R, Negrin JA, Margouleff D. Scintigraphic evaluation of postoperative complications of laparoscopic cholecystectomy. J Nucl Med. 1991;32:1910–1.
25. Weissmann HS, Byun KJ, Freeman LM. Role of Tc-99m IDA scintigraphy in the evaluation of hepatobiliary trauma. Semin Nucl Med. 1983;13:199–222.
26. Majd M, Reba RC, Altman RP. Effect of phenobarbital on 99mTc-IDA scintigraphy in the evaluation of neonatal jaundice. Semin Nucl Med. 1981;11:194–204.
27. Lee CH, Wang PW, Lee TT, Tiao MM, Huang FC, Chuang JH, Shieh CS, Cheng YF. The significance of functioning gallbladder visualization on hepatobiliary scintigraphy in infants with persistent jaundice. J Nucl Med. 2000;41:1209–13.
28. Kianifar HR, Tehranian S, Shojaei P, Adinehpoor Z, Sadeghi R, Kakhki VR, Keshtgar AS. Accuracy of hepatobiliary scintigraphy for differentiation of neonatal hepatitis from biliary atresia: systematic review and meta-analysis of the literature. Pediatr Radiol. 2013;43:905–19.
29. Hasegawa Y, Nakano S, Ibuka K, Hashizume T, Noguchi A, Sasaki Y, Imaoka S, Fujita M, Kawamoto S, Kasugai H, et al. Specific diagnosis of hepatocellular carcinoma by delayed hepatobiliary imaging. Cancer. 1986;57:230–6.
30. Lee VW, O'Brien MJ, Devereux DF, Morris PM, Shapiro JH. Hepatocellular carcinoma: uptake of 99mTc-IDA in primary tumor and metastasis. AJR. 1984;143:57–61.
31. Calvet X, Pons F, Bruix J, Bru C, Lomena F, Herranz R, Brugera M, Faus R, Rodes J. Technetium-99m DISIDA hepatobiliary agent in diagnosis of hepatocellular carcinoma: relationship between detectability and tumor differentiation. J Nucl Med. 1988;29:1916–20.
32. Drane WE, Krasicky GA, Johnson DA. Radionuclide imaging of primary tumors and tumor-like conditions of the liver. Clin Nucl Med. 1987;12:569–82.
33. Lee VW, O'Brien MJ, Morris PM, Devereux DF, Shapiro JH. The specific diagnosis of hepatocellular carcinoma by scintigraphy. Multiple radiotracer approach. Cancer. 1985;56:25–36.
34. Middleton ML. Scintigraphic evaluation of hepatic mass lesions: emphasis on hemangioma detection. Semin Nucl Med. 1996;26:4–15.

35. Chilton HM, Brown ML, Swanson DP, Chilton HM, Thrall JH. Radiopharmaceuticals for abdominal and gastrointestinal imaging: reticuloendothelial, hepatobiliary, and intestinal. In: Pharmaceuticals in Medical Imaging. New York, NY: Macmillan Publishing Co., Inc.; 1990. p. 462–500.
36. Metter DF, Elman S, Shreve PD, Majd M, Servaes S, Shore RM, Williams JL. ACR–SPR practice parameter for the performance of liver and spleen scintigraphy. ACR–SPR. 2015;2015:1–8.
37. Metter DF, Fig LM, Gelfand MJ, Shreve PD, Binkovitz LA, Majd M, Parisi MT, Spottswood SE, Balon HR, Powsner RA. ACR–SNM–SPR practice guideline for the performance of liver and spleen scintigraphy. ACR–SNM–SPR. 2010;2010:1–5.
38. Yammine JN, Yatim A, Barbari A. Radionuclide imaging in thoracic splenosis and a review of the literature. Clin Nucl Med. 2003;28:121–3.
39. Gore RM, Newmark GM, Thakrar KH, Mehta UK, Berlin JW. Hepatic incidentalomas. Radiol Clin North Am. 2011;49:291–322.
40. Waxman AD. Scintigraphic evaluation of diffuse hepatic disease. Semin Nucl Med. 1982;12:75–88.
41. McClees EC, Gedgaudas-McClees RK. Screening for diffuse and focal liver disease: the case for hepatic scintigraphy. J Clin Ultrasound. 1984;12:75–81.
42. Hoefs JC, Sheikh MY, Guerrero H, Milne N. Factors affecting the quantitative liver-spleen scan in normal individuals. Dig Dis Sci. 2005;50:283–9.
43. Geslien GE, Pinsky SM, Poth RK, Johnson MC. The sensitivity and specificity of 99mTc-sulfur colloid liver imaging in diffuse hepatocellular disease. Radiology. 1976;118:115–9.
44. Kim EE. Focal splenic defect. Semin Nucl Med. 1979;9:320–1.
45. Baker MK, Schauwecker DS, Wenker JC, Kopecky KK. Nuclear medicine evaluation of focal fatty infiltration of the liver. Clin Nucl Med. 1986;11:503–6.
46. Lisbona R, Rush CL, Derbekyan V, Novales-Diaz JA. Radiocolloid liver imaging in hepatic steatosis. Clin Nucl Med. 1986;11:183–7.
47. Alderson PO, Adams DF, McNeil BJ, Sanders R, Siegelman SS, Finberg HJ, Hessel SJ, Abrams HL. Computed tomography, ultrasound, and scintigraphy of the liver in patients with colon or breast carcinoma: a prospective comparison. Radiology. 1983;149:225–30.
48. Davis LP, McCarroll K. Correlative imaging of the liver and hepatobiliary system. Semin Nucl Med. 1994;24:208–18.
49. Fawcett HD, Sayle BA. SPECT versus planar liver scintigraphy: is SPECT worth it? J Nucl Med. 1989;30:57–9.
50. Welch TJ, Sheedy PF 2nd, Johnson CM, Stephens DH, Charboneau JW, Brown ML, May GR, Adson MA, McGill DB. Focal nodular hyperplasia and hepatic adenoma: comparison of angiography, CT, US, and scintigraphy. Radiology. 1985;156:593–5.
51. Lubbers PR, Ros PR, Goodman ZD, Ishak KG. Accumulation of technetium-99m sulfur colloid by hepatocellular adenoma: scintigraphic-pathologic correlation. AJR. 1987;148:1105–8.
52. Rubin RA, Lichtenstein GR. Hepatic scintigraphy in the evaluation of solitary solid liver masses. J Nucl Med. 1993;34:697–705.
53. Dickson AM. The focal hepatic hot spot sign. Radiology. 2005;237:647–8.
54. Tetalman MR, Kusumi R, Gaughran G, Baba N. Radionuclide liver spots: indicator of liver disease or a blood flow phenomenon. AJR. 1978;130:291–6.
55. Muramatsu T, Miyamae T, Mashimo M, Suzuki K, Kinoshita S, Dohi Y. Hot spots on liver scans associated with superior or inferior vena caval obstruction. Clin Nucl Med. 1994;19:622–9.
56. Meindok H, Langer B. Liver scan in Budd-Chiari syndrome. J Nucl Med. 1976;17:365–8.
57. Shreiner DP, Barlai-Kovach M. Diagnosis of alcoholic cirrhosis with the right-to-left hepatic lobe ratio: concise communication. J Nucl Med. 1981;22:116–20.
58. Armas RR. Clinical studies with spleen-specific radiolabeled agents. Semin Nucl Med. 1985;15:260–75.
59. Massey MD, Stevens JS. Residual spleen found on denatured red blood cell scan following negative colloid scans. J Nucl Med. 1991;32:2286–7.
60. Oates E, Austin JM, Becker JL. Technetium-99m-sulfur colloid SPECT imaging in infants with suspected heterotaxy syndrome. J Nucl Med. 1995;36:1368–71.
61. Ishak KG, Rabin L. Benign tumors of the liver. Med Clin North Am. 1975;59:995–1013.
62. Nelson RC, Chezmar JL. Diagnostic approach to hepatic hemangiomas. Radiology. 1990;176:11–3.
63. Middleton ML, Milstein DM, Freeman LM, Freeman LM. Hepatic mass lesions: scintigraphic update with emphasis on hemangioma detection. In: Nuclear medicine annual 1994. New York, NY: Raven Press, Ltd.; 1994. p. 55–90.
64. Kudo M, Ikekubo K, Yamamoto K, Ibuki Y, Hino M, Tomita S, Komori H, Orino A, Todo A. Distinction between hemangioma of the liver and hepatocellular carcinoma: value of labeled RBC-SPECT scanning. AJR Am J Roentgenol. 1989;152:977–83.
65. Ziessman HA, Silverman PM, Patterson J, Harkness B, Fahey FH, Zeman RK, Keyes JW Jr. Improved detection of small cavernous hemangiomas of the liver with high-resolution three-headed SPECT. J Nucl Med. 1991;32:2086–91.
66. Tsai CC, Yen TC, Tzen KY. The value of Tc-99m red blood cell SPECT in differentiating giant cavernous hemangioma of the liver from other liver solid masses. Clin Nucl Med. 2002;27:578–81.
67. Rabinowitz SA, McKusick KA, Strauss HW. 99mTc red blood cell scintigraphy in evaluating focal liver lesions. AJR. 1984;143:63–8.
68. Ginsberg F, Slavin JD Jr, Spencer RP. Hepatic angiosarcoma: mimicking of angioma on three-phase technetium-99m red blood cell scintigraphy. J Nucl Med. 1986;27:1861–3.
69. Khandani AH, Wahl RL. Applications of PET in liver imaging. Radiol Clin North Am. 2005;43:849–60.

70. Bombardieri E, Aliberti G, de Graaf C, Pauwels E, Crippa F. Positron emission tomography (PET) and other nuclear medicine modalities in staging gastrointestinal cancer. Semin Surg Oncol. 2001;20:134–46.
71. Pelletier-Galarneau M, Martineau P, Zuckier LS, Pham X, Lambert R, Turpin S. (18)F-FDG-PET/CT imaging of thoracic and extrathoracic tuberculosis in children. Semin Nucl Med. 2017;47:304–18.
72. Rosenthal SA, Yung EY-K, Zaki BI, Salem R, Coldwell DM, Murthy R, Nutting CW. ACR–SIR practice parameter for radioembolization with microsphere brachytherapy device (RMBD) for treatment of liver malignancies. edited by American College of Radiology (ACR), and SIR; 2014.
73. Civelek AC, Sitzmann JV, Chin BB, Venbrux A, Wagner HN Jr, Grochow LB. Misperfusion of the liver during hepatic artery infusion chemotherapy: value of preoperative angiography and postoperative pump scintigraphy. AJR. 1993;160:865–70.
74. Thrall JH. Hepatic arterial chemotherapy: pharmacokinetic rationale and radionuclide perfusion imaging. Nucl Med Annu. 1984;1984:211–26.
75. Drane WE. Nuclear medicine techniques for the liver and biliary system. Update for the 1990s. Radiol Clin North Am. 1991;29:1129–50.
76. Vogel SB, Drane WE, Ros PR, Kerns SR, Bland KI. Prediction of surgical resectability in patients with hepatic colorectal metastases. Ann Surg. 1994;219:508–14; discussion 514–506.
77. Bozkurt MF, Salanci BV, Ugur O. Intra-arterial radionuclide therapies for liver tumors. Semin Nucl Med. 2016;46:324–39.
78. Salem R, Lewandowski RJ, Atassi B, Gordon SC, Gates VL, Barakat O, Sergie Z, Wong CY, Thurston KG. Treatment of unresectable hepatocellular carcinoma with use of 90Y microspheres (TheraSphere): safety, tumor response, and survival. J Vasc Interv Radiol. 2005;16:1627–39.
79. Biocompatibles UK Limited. TheraSphere® Yttrium-90 glass microspheres; 2014.
80. Murthy R, Nunez R, Szklaruk J, Erwin W, Madoff DC, Gupta S, Ahrar K, Wallace MJ, Cohen A, Coldwell DM, Kennedy AS, Hicks ME. Yttrium-90 microsphere therapy for hepatic malignancy: devices, indications, technical considerations, and potential complications. Radiographics. 2005;25(Suppl 1):S41–55.
81. Sirtex Medical Limited. SIR-Spheres® microspheres (Yttrium-90 Microspheres); 2014.
82. Ahmad M, Witztum KF, Fletcher JW, Hendershott LR, Klos D, George EA, Donati RM. Xenon-133 accumulation in hepatic steatosis. J Nucl Med. 1977;18:881–5.
83. Lisbona R, Mishkin S, Derbekyan V, Novales-Diaz JA, Roy A, Sanders L. Role of scintigraphy in focally abnormal sonograms of fatty livers. J Nucl Med. 1988;29:1050–6.
84. Shih WJ, Shih GL, Milan PP. Xenon 133 ventilation studies as an alternative for detecting and quantifying fatty infiltration of the liver. Radiographics. 2010;30:958–9; author reply 959–960
85. Kaltsas G, Rockall A, Papadogias D, Reznek R, Grossman AB. Recent advances in radiological and radionuclide imaging and therapy of neuroendocrine tumours. Eur J Endocrinol. 2004;151:15–27.
86. Pashankar FD, O'Dorisio MS, Menda Y. MIBG and somatostatin receptor analogs in children: current concepts on diagnostic and therapeutic use. J Nucl Med. 2005;46(Suppl 1):55S–61S.
87. Pfluger T, Piccardo A. Neuroblastoma: MIBG imaging and new tracers. Semin Nucl Med. 2017;47:143–57.
88. Pfannenberg AC, Eschmann SM, Horger M, Lamberts R, Vonthein R, Claussen CD, Bares R. Benefit of anatomical-functional image fusion in the diagnostic work-up of neuroendocrine neoplasms. Eur J Nucl Med Mol Imaging. 2003;30:835–43.
89. Jacobsson H, Jonas E, Hellstrom PM, Larsson SA. Different concentrations of various radiopharmaceuticals in the two main liver lobes: a preliminary study in clinical patients. Journal of gastroenterology. 2005;40:733–8.
90. Ezuddin S, Fragkaki C. MIBG and FDG PET findings in a patient with malignant pheochromocytoma: a significant discrepancy. Clin Nucl Med. 2005;30:579–81.
91. Drane WE. Scintigraphic techniques for hepatic imaging. Update for 2000. Radiol Clin North Am. 1998;36:309–18.
92. Belhocine T, Foidart J, Rigo P, Najjar F, Thiry A, Quatresooz P, Hustinx R. Fluorodeoxyglucose positron emission tomography and somatostatin receptor scintigraphy for diagnosing and staging carcinoid tumours: correlations with the pathological indexes p53 and Ki-67. Nucl Med Commun. 2002;23:727–34.
93. Hofman MS, Lau WF, Hicks RJ. Somatostatin receptor imaging with 68Ga DOTATATE PET/CT: clinical utility, normal patterns, pearls, and pitfalls in interpretation. Radiographics. 2015;35:500–16.
94. Agrawal K, Esmail AA, Gnanasegaran G, Navalkissoor S, Mittal BR, Fogelman I. Pitfalls and limitations of radionuclide imaging in endocrinology. Semin Nucl Med. 2015;45:440–57.
95. Lomas F, Dibos PE, Wagner HN Jr. Increased specificity of liver scanning with the use of 67 gallium citrate. N Engl J Med. 1972;286:1323–9.
96. Larson SM, Rasey JS, Allen DR, Nelson NJ, Grunbaum Z, Harp GD, Williams DL. Common pathway for tumor cell uptake of gallium-67 and iron-59 via a transferrin receptor. J Natl Cancer Inst. 1980;64:41–53.
97. Hauser MF, Alderson PO. Gallium-67 imaging in abdominal disease. Semin Nucl Med. 1978;8:251–70.
98. Suzuki T, Matsumoto Y, Manabe T, Honjo I, Proceedings HK. Serum alpha-fetoprotein and Ga67 citrate uptake in hepatoma. AJR. 1974;120:627–33.
99. Rosenbaum SJ, Stergar H, Antoch G, Veit P, Bockisch A, Kuhl H. Staging and follow-up of gastrointestinal tumors with PET/CT. Abdom Imaging. 2006;31:25–35.